Mon. Not. R. Astron. Soc. **000**, 1–19 (2002) Printed 4 March 2009 (MN LATEX style file v2.2)

Hydrodynamical simulations of Galactic fountains II: evolution of multiple fountains

C. Melioli,[1⋆] F. Brighenti[2], A.D'Ercole[1] and E.M. de Gouveia Dal Pino[3]
[1] *INAF-Osservatorio Astronomico di Bologna, via Ranzani 1, 40126 Bologna, Italy*
[2] *Dipartimento di Astronomia, Università di Bologna, via Ranzani 1, 40126 Bologna, Italy*
[3] *IAG, Universidade de São Paulo, Rua do Matão 1226, 05508-090 São Paulo, Brazil*

Accepted ... Received ...; in original form ...

ABSTRACT
The ejection of gas out of the disk in late-type galaxies is related to star formation and is mainly due to the explosion of Type II supernovae. In a previous paper, we considered the evolution of a single Galactic fountain, that is, a fountain powered by a single supernova cluster. Using 3D hydrodynamical simulations, we studied in detail the fountain flow and its dependence with several factors, such as the Galactic rotation, the distance to the Galactic center, and the presence of a hot gaseous halo. As a natural follow-up, the present paper investigates the dynamical evolution of multiple generations of fountains generated by ~ 100 OB associations. We have considered the observed size-frequency distribution of young stellar clusters within the Galaxy in order to appropriately fuel the multiple fountains in our simulations. Most of the results of the previous paper have been confirmed, like for example the formation of intermediate velocity clouds above the disk by the multiple fountains. Also, the present work confirms the localized nature of the fountain flows: the freshly ejected metals tend to fall back close to the same Galactocentric region where they are delivered. Therefore, the fountains do not change significantly the radial profile of the disk chemical abundance. The multiple fountains simulations also allowed to consistently calculate the feedback of the star formation on the halo gas. We found that the hot gas gains about 10 % of all the SNII energy produced in the disk. Thus, the SN feedback more than compensate for the halo radiative losses and allow for a quasi steady-state disk-halo circulation to exist. Finally, we have also considered the possibility of mass infall from the intergalactic medium and its interaction with the clouds that are formed by the fountains. Though our simulations are not suitable to reproduce the slow rotational pattern that is typically observed in the halos around the disk galaxies, they indicate that the presence of an external gas infall may help to slow down the rotation of the gas in the clouds and thus the amount of angular momentum that they transfer to the coronal gas, as previously suggested in the literature.

Key words:

1 INTRODUCTION

Galactic fountains (GFs) are believed to occur in the Milky Way as well as in the other disk galaxies. A GF takes place when the Type II supernovae (SNe II) belonging to an OB association are sufficiently numerous to create a superbubble and to drive its expansion above the scale height of the gaseous disk (Shapiro & Field 1976; Bregman 1980; Kahn 1981). As the break out occurs (Mac Low et al. 1989; Koo & McKee 1992), the gas heated by the SNe II falls back to the Galactic plane as cold gas, mostly concentrated in clouds formed through thermal instabilities.

The GF mechanism is thought to be linked to a number of issues which have been discussed in some detail in Melioli et al. (2008, thereafter Paper I). Here we briefly recall them: *i*) the formation of the observed thick H I layer having a mass of 1/10 of the total H I, and rotating with velocity about 20-50 km s^{-1} smaller than that of the gas on the plane; *ii*) the presence of high velocity clouds (HVCs) and/or intermediate velocity clouds (IVCs). It is important to understand whether these clouds are formed by GFs, or represent external gas accreting on the disk (Sancisi et al.

⋆ E-mail: claudio.melioli@oabo.inaf.it; fabrizio.brighenti@unibo.it; annibale.dercole@oabo.inaf.it; dalpino@astro.iag.usp.br

2008); *iii*) the presence of giant holes in the H I disk of many galaxies, which can be produced by associations of O and B stars exploding in a correlated fashion and giving rise to superbubbles; *iv*) the chemical evolution of the Galaxy, as in principle GFs might be able to move SN II ejecta relatively far from the place where they have been produced, affecting the gradients of α-elements; *v*) the diffuse, soft ($T \lesssim 1$ keV), extraplanar X-ray emission detected in some spiral galaxies which is due to hot gas extending up to 10 kpc above the galactic disk. This gas is most likely blown out by star forming regions in the disk, as the X-ray luminosity correlates with the star formation rate and the hot gas is oxygen rich, a signature of SN II enrichment.

Given the richness of the phenomena involved in the GFs, a number of papers has been devoted to this argument. A detailed analytical description of the motion of a fluid element in a GF from the rotating disk to the halo and back, predicting the location where it would return on the disk was first presented by Kahn (1991) and Kahn & Brett (1993). de Avillez (2000) and de Avillez & Berry (2001) performed several 3D hydrodynamical simulations of the gas in the Milky Way in order to account for the collective effects of supernovae on the structure of the interstellar medium (ISM). In particular, de Avillez (2000) discussed in detail for the first time the fraction of material that results in the formation of IVCs. More recently, further 3D MHD simulations were carried out by de Avillez & Breitschwerdt (2005). They found that gas transport into the halo as well as the mean volume filling factor of the hot phase in the disk is not significantly affected by the presence of a initial disk parallel magnetic field (see also Tomisaka 1998). In order to reach a high spatial resolution, all these simulations consider only small disk regions (typically 1 kpc$^2\times$ 10 kpc) and assume plane parallel stratified ISM. Korpi et al. (1999) have included in their 3D numerical simulations the effects of the differential rotation and the magnetic field of the galactic disk, but again considered a small computational domain (500 pc^2 $\times$ 1 kpc). In all the simulations above any dependence of the variables with the Galactocentric distance is neglected. The lack of an extended grid makes the entire development of a disk-halo-disk cycle very difficult to follow because part of the mass is lost through the grid boundaries.

The simulations by Fraternali & Binney (2006) followed a different strategy. They considered the whole Galaxy and calculated the orbits of gas clouds assumed to be like bullets ejected (by SNe II) from the disk that move ballistically up into the halo and then return to the disk. However, hydrodynamical effects have been essentially neglected in these models.

In order to study the large scale motion of the ISM and the halo gas and follow the complete dynamical and thermal evolution of the gas lifted by the galactic fountains, the whole, differentially rotating Galaxy must be considered. In Paper I we have presented 3D hydrodynamical simulations of the evolution of a single GF (SGF), i.e. a fountain generated by only one OB association with 100 SNe. There, we investigated the influence on the SGF dynamics of several factors, such as the Galactocentric distance, the Galactic rotation, and the presence of a gaseous halo and/or a disk neutral hydrogen layer. We have found that a SGF may eject material up to $\sim$ 2 kpc before it collapses back in the disk, mostly in form of dense, cold clouds and filaments, with velocities which are compatible with those of the IVCs. Contrary to the common expectation, the gas lifted up by the SGF tends to move toward the centre rather than toward the outskirts of the disk because part of its angular momentum is transferred to the halo and/or the upper layers of the disk. However, most of the GF gas falls back on the disk within a radial distance $\Delta R \sim 0.5$ kpc from the place where the fountain originated. This localized circulation of disk gas agrees with recent chemical models of the Milky Way which assume that the SNII metals enrich only the local ISM. (Cescutti et al. 2007).

The present paper is devoted to multiple Galactic fountains (MGFs) - i.e. fountains generated by multiple OB associations - in which the gas flow is due to the continuous star formation in the Galactic disk. Thus, this paper represents a natural extension of the analysis of Paper I on single fountains. To keep the computational costs under reasonable limits, we have followed in detail only a limited volume of the Galaxy where the MGF occurs; the remaining Galactic volume was mapped at a lower resolution. Although a very accurate description of the different ISM phases (as in de Avillez 2000; de Avillez & Berry 2001) is hampered by the limited resolution resulting from our approach, the global evolution of the fountains can be satisfactorily calculated. We neglected the effect of magnetic field; as shown by the aforementioned papers by Kahn (1991); Kahn & Brett (1993); de Avillez & Breitschwerdt (2005) it does not strongly affect the global fountain dynamics.

An important motivation to run simulations of MGFs is to investigate the mass and energy exchange between the star forming disk and the hot gaseous halo surrounding the Galaxy. The efficiency of the SN feedback is a key, yet poorly understood issue in theories of galactic star formation, as we will outline later (c.f. Navarro & Steinmetz 1997). We find that a non-negligible fraction of the SN energy is indeed injected in the halo (Section 3.4).

A further reason to consider multiple fountains is to explore the interaction with external gas infalling onto the disk. Indeed, such gas is needed in current galaxy evolution models in order to maintain star formation rates similar to those observed in normal spiral galaxies (e.g. Takeuchi & Hirashita 2000; Semelin & Combes 2002), as well as to explain the observed patterns in the chemical evolution of the Milky Way (Chiappini 2002; Geiss et al. 2002). Fraternali et al. (2007) detected inflowing HI clouds in the nearby spiral galaxies NGC 891 and NGC 2403. They argue that these clouds are a clue to a substantial and otherwise mostly hidden halo gas accretion interacting with GFs. While the required accretion rate is comparable to the star formation rate, the infalling gas must have low angular momentum (Fraternali & Binney 2006).

In the following sections, we outline the basic characteristics and the setup of our numerical model (Sec. 2), then examine a reference model for the investigation of multiple fountains (MGFs) formation in the Galaxy at a distance of 8.4 kpc from the galactic centre (Sec. 3) and compare these results with a model where the MGFs occur at $R = 4.5$ kpc (Sec. 4). Finally, in Sec. 5, we consider the interaction of MGFs with infalling gas from the intergalactic medium and in Sec. 6, we draw our conclusions.

2 THE MODEL

The model of the Milky Way, as well as the assumptions relative to the SN II explosions belonging to single associations, are fully described in Paper I. Here we briefly recapitulate them and discuss in detail how we take into account the stellar explosions occurring in different OB associations.

2.1 The Galaxy model

The ISM in our model is made up of three components - namely molecular (H_2), neutral (H I) and ionized (H II) hydrogen - all following the spatial distribution given by Wolfire et al. (2003) (see also Paper I). The ISM is initially set in rotational equilibrium in the Galactic gravitational potential due to the summation of the dark matter halo, the bulge and the disk contributions, as described by Navarro et al. (1996), Hernquist (1990), and by a flattened King profile (Brighenti & Mathews 1996), respectively. A hot isothermal gas halo in hydrostatic equilibrium with the Galactic potential well is also added. This halo has a central density $\rho_{0,\rm h} = 2.17 \times 10^{-27}$ g cm^{-3} and a temperature $T_{\rm h} = 7 \times 10^6$ K.

2.2 Supernovae explosions

2.2.1 Single associations

It is known that the great majority of the massive stars form in clusters (e.g. Ward-Thompson 2002, and references therein). In Paper I, we defined a "single fountain" as a fountain powered by the SNe II present in a single cluster[1]. The OB association driving the fountain was assumed to be totally housed inside a single zone of the highest resolution level of our adaptive grid (see section 2.3). The SNe II do not explode all at the same time because of the different mass of their progenitors. Thus the energy and the mass delivered by all the explosions are released over a time interval of Δt=30 Myr (the lifetime of an 8 $M_\odot$ star, which is the least massive SN II progenitor). The stellar explosions inject mass and energy at the rates $\dot{M} = \mathcal{R} M_{\rm ej}$ and $L_{\rm w} = \mathcal{R} E_0$, respectively. Here $M_{\rm ej} = 16\ M_\odot$ and $E_0 = 10^{51}$ erg are the mean mass and energy released by a single explosion, respectively; $\mathcal{R} = N_{\rm SN}/\Delta t$ is the SN II rate, and $N_{\rm SN}$ is the total number of SN II explosions occurring in the association. $L_{\rm w}$ represents the mechanical luminosity of the wind driven by the SNe II and inflating a superbubble. If the luminosity is larger than a critical value $L_{\rm cr}$, the superbubble breaks out of the disk forming a chimney in the ISM and gives rise to the GF (cf. Paper I and references therein). In section 2.3 we describe as $L_{\rm w}$ is implemented into the numerical grid.

2.2.2 Multiple associations

At the observed rate (see below), several SGFs may occur sufficiently close to each other in time and space to mutually interact. This interaction obviously modifies the general dynamics of the SN II ejecta of each single fountain. Following with an adequate spatial resolution all the SN II explosions occurring in the whole disk is beyond our current computational capabilities. Thus, throughout the simulations of multiple fountains, we focus in particular on a circular area (hereafter referred to as the "active area") of the Galactic disk of 8 kpc^2 which is resolved up to the maximum level of grid refinement (this finest grid extends vertically up to $z = 3.2$ kpc). We allow the SNe II to occur only in this area over a period $T = 200$ Myr. It must be emphasized that the star formation rate (and the associated SN rate) is not computed self-consistently with the gas evolution. Instead, we assume a mean SN rate adequately scaled from the rate 1.4×10^{-2} yr^{-1} relative to the whole Galaxy (Cappellaro et al. 1997). It turns out that during the time T of our simulations $N_{\rm tot} = 4.2 \times 10^4$ SNe II are expected to explode in the active area of the Galactic disk (see, however, the end of this section).

Let us assume $f(N_{\rm SN}) dN_{\rm SN}$ to be the number of stellar clusters with a number of supernova progenitors between $N_{\rm SN}$ and $N_{\rm SN} + dN_{\rm SN}$. $f(N_{\rm SN})$ follows a power law distribution (Higdon & Lingenfelter 2005),

$$f(N_{\rm SN}) \propto N_{\rm SN}^{-2}, \qquad N_{\rm min} < N_{\rm SN} < N_{\rm max}. \tag{1}$$

We normalize $f(N_{\rm SN})$ in order to get

$$\int_{N_{\rm min}}^{N_{\rm max}} N_{\rm SN} f(N_{\rm SN}) dN_{\rm SN} = N_{\rm tot}. \tag{2}$$

This normalization can be done once $N_{\rm min}$ and $N_{\rm max}$ have been chosen (see below in this section).

We choose bins in $N_{\rm SN}$ such that

$$\int_{N_{\rm SN}^i}^{N_{\rm SN}^{i+1}} f(N_{\rm SN}) dN_{\rm SN} = 1; \tag{3}$$

we then assume that such a cluster contains $0.5(N_{\rm SN}^i + N_{\rm SN}^{i+1})$ SNe II. Clearly, for $i = 1$ we have $N_{\rm SN}^1 = N_{\rm min}$.

Once obtained the number and the richness of the clusters, we place them within the active area. This is made associating randomly to each i-th cluster a position P_j within the active area and a time t_j in the range $0 < t_j < T$. As the time proceeds, the supernovae belonging to the i-th cluster start to explode at P_j at the time t_j (and continue to explode for 30 Myr, as outlined in section 2.2.1). The sequel of the SN II "bursts" is shown in Fig. 1. The energy provided by the i-th burst is $E_0 N_{\rm SN}^i$.

To choose $N_{\rm min}$ and $N_{\rm max}$, we simply assume $N_{\rm max}$=2000 from Higdon & Lingenfelter (2005). With regard to $N_{\rm min}$, although in principle it can be as low as $N_{\rm min} = 1$, we assume $N_{\rm min} = 30$. At a distance of $R = 8.5$ kpc, which is the Galactocentric distance of the centre of the active area in our reference model (cf. section 3), GFs can form only when $L_{\rm w} \gtrsim L_{\rm cr} = 3 \times 10^{37}$ erg s^{-1} (cf. Paper I), that is for clusters richer than $N_{\rm SN} \gtrsim 30$. In order to capture the physics of interest here, we have thus adopted $N_{\rm min} = 30$. As a *caveat*, we stress that with this choice of $N_{\rm min}$ the actual number of SN II explosions occurring after $T = 200$ Myr is nearly $N_{\rm tot}/2$, i.e., half of those expected. Although this is not important from a dynamical point of view, it influences the amount of metals set in circulation by the fountains. We have to remember this when discussing the chemical pollution of the disk.

[1] For the sake of simplicity, by SNe II we mean here all the core collapse explosions.

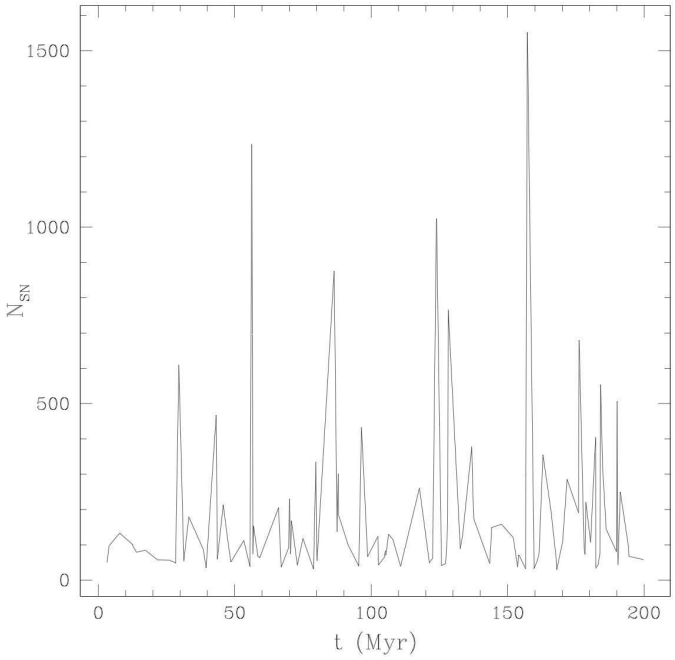

Figure 1. Temporal histogram of the sequence of stellar clusters fuelling our models of multiple Galactic fountains. The y-axis reports the number of SNe II of each cluster; the x-axis shows the time in Myr.

2.3 Numerical Setup

We use a modified version of the numerical adaptive mesh refinement (AMR) YGUAZUa hydrodynamical code (Raga et al. 2000, 2002). The radiative losses are calculated assuming solar abundances and by using non-equilibrium ionization species abundances (for HI, HII, CII, CIII, CIV, OI, OII and OIII) when $T \geqslant 10^6$ K. For higher temperatures, where the collisional ioniziation equilibrium is often a good approximation, we use an equilibrium cooling function taken from Sutherland & Dopita (1993). More details can be found in Paper I. We enforce the maximum grid resolution only within the active volume defined in the previous section (given the symmetry of the problem, our computational volume encompasses only the "upper" half of the Galaxy). As a reasonable compromise between the need of a large active surface and a good spatial resolution within it, we chose an area of 8 kpc^2 and a minimum mesh size of 50 pc. The other three coarser grid levels have mesh sizes of 100 pc, 200 pc and 400 pc, respectively.

The rate of mass and energy injection by SNe II belonging to every single association is described in section 2.2.1. Because the numerical grid is at rest in space while the Galaxy rotates, each OB association occurring in the active area moves along a circle on the $z = 0$ plane. At each time we place the energy and mass sources in the numerical cell of the finest grid transited by the association at that time. We stress that while we assume that all the OB association are located at $z = 0$, SNII progenitors are observed to have a vertical distribution with scale height of ~ 100 pc. As our finest grid has a size of 50 pc, in order to investigate the effect of the vertical position on the fountain evolution we must locate OB associations only two zones above the equatorial plane. Such a small displacement is not expected to generate appreciable differences in the calculated flow evolution.

3 THE REFERENCE MODEL

In this section we discuss the reference model (RM), in which the active area is centred at the Galactocentric distance $R =$ 8.4 kpc.

3.1 ISM in the disk

Figure 2 shows the time evolution of the gas column density of the ISM of the disk along the direction perpendicular to the Galactic plane (the z-direction). The two dashed circles in the panels delimit the region within which the active area evolves as the Galaxy rotates. There are several cavities whose lifetime is given by the duration of the SN activity in each association (~ 30 Myr) added to the time needed for the replenishment to occur at the end of such activity. The replenishment time is approximately given by $t_{\rm rep} \sim r_{\rm c}/c$, where $r_{\rm c}$ is the maximum radius attained by the cavities, and c is the sound speed of the ambient medium. It turns out that $r_{\rm c} \sim 0.7$ kpc for the largest cavities, while $c \sim 2 \times 10^6$ cm s^{-1}, and thus $t_{\rm rep} \sim 37$ Myr. In conclusion, the lifetime of the holes into the disk ISM is $\lesssim 70$ Myr. This lifetime and the occurrence rate of the OB associations both conspire to avoid a substantial overlapping of the holes and the area of interest is never totally deprived of its ISM. Given the differential rotation of the Galaxy, the holes become elongated with positive pitch angles (angle between the major axis of the hole and the tangent to a circle at that galactic radius), as described by the models of Palous et al. (1990). As a further effect of the disk differential rotation, the holes created at earlier times lag behind the recent ones, tending to form a sort of queue. This latter effect, however, arises because our active region is limited. Had the active area covered the whole disk, its appearance would be similar to NGC 2403 (Fraternali et al. 2002) and other typical spirals.

In a recent paper Boomsma et al. (2008) presented a detailed study of the H I holes and HVCs in the spiral galaxy NGC 69456. It is interesting to compare our results to their findings. Boomsma et al. (2008) evaluate an average radius of the holes of 0.6 kpc and a maximum lifetime of about 80 Myr; both these figures are very close to the values obtained in our simulation. Those authors also find that the hole covering factor drops sharply toward the smallest galactic radii, an effect ascribed to the drop of the H I column density as well as to the stronger shear which shortens the hole lifetimes. Smaller dimensions and shorter lifetimes at smaller radii are also met in our models, and we find that the reason is given by the larger pressure of the ambient gas which contrasts the bubble expansion and favours the hole replenishment (cf. sect. 4). Finally, Boomsma et al. (2008) estimate an upper limit of about 10^7 M$_\odot$ for the average H I mass missing from each hole. In our simulation we have 3-5 holes present at every time (cf. Fig. 2), while the disk gas lifted at any time is a few 10^7 M$_\odot$ (cf. sect. 3.4), thus giving roughly 5×10^6 M$_\odot$ per hole, consistently with the upper limit estimated by Boomsma et al. (2008). In conclusion, despite our one-fluid approximation of the multi-phase ISM

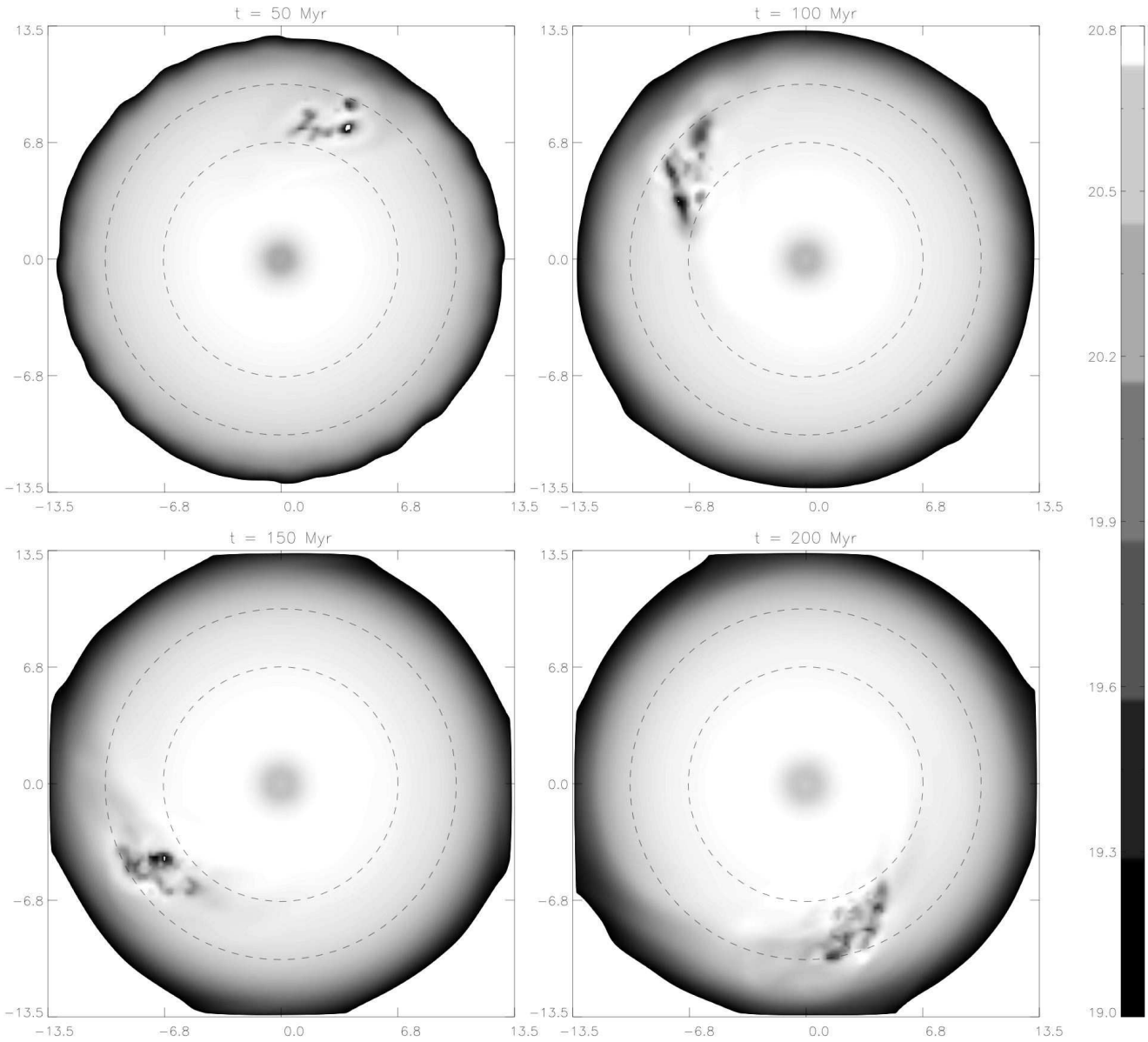

Figure 2. Face-on view of the active area for the reference model (RM). Column density along the z direction of the ISM of the Galactic disk at several times. The two superimposed dashed circles have radii of 6.8 kpc and 10 kpc and they delimit the ring within which the active disk area moves. The logarithmic column density scale is given in cm^{-2} and the spatial scale along the x and y directions is in kpc.

and the galactic model tailored on the Milky Way rather than on NGC 69456, our results are in encouraging agreement with the observational data.

3.2 Gas circulation

Figure 3 represents a sort of tomography at different times of the column density of the SN II ejecta along the z direction. The total column densities are shown in the right panels; the left and right panels illustrate the contributions of ejecta located below and above $z = 800$ pc (the height at which the disk/halo transition is located for a radial distance of $R = 8.4$ kpc), respectively. The dense spots present in the first column of the panels are due to recent SN explosions (see, for example, the top-left panel). Instead, the more structured distribution visible in the middle column is due to ejecta trapped and condensed within clouds forming at larger z from the lifted disk gas which suffers thermal instability and cools down to $T = 10^4$ K (the minimum temperature allowed in our simulations). These clouds are characterized by large column densities, and are visible in Fig. 3 as red spots.

The cold, dense gas must eventually fall back onto the disk. Figure 4 shows the column density of the clouds with negative vertical velocity (the cloud gas is selected as gas with $T \leqslant 5 \times 10^4$ K). This figure clearly demonstrates how the gas lifted by the fountains falls back remaining mostly within the ring of the disk in which the active area is located. This result confirms what was found in Paper I and

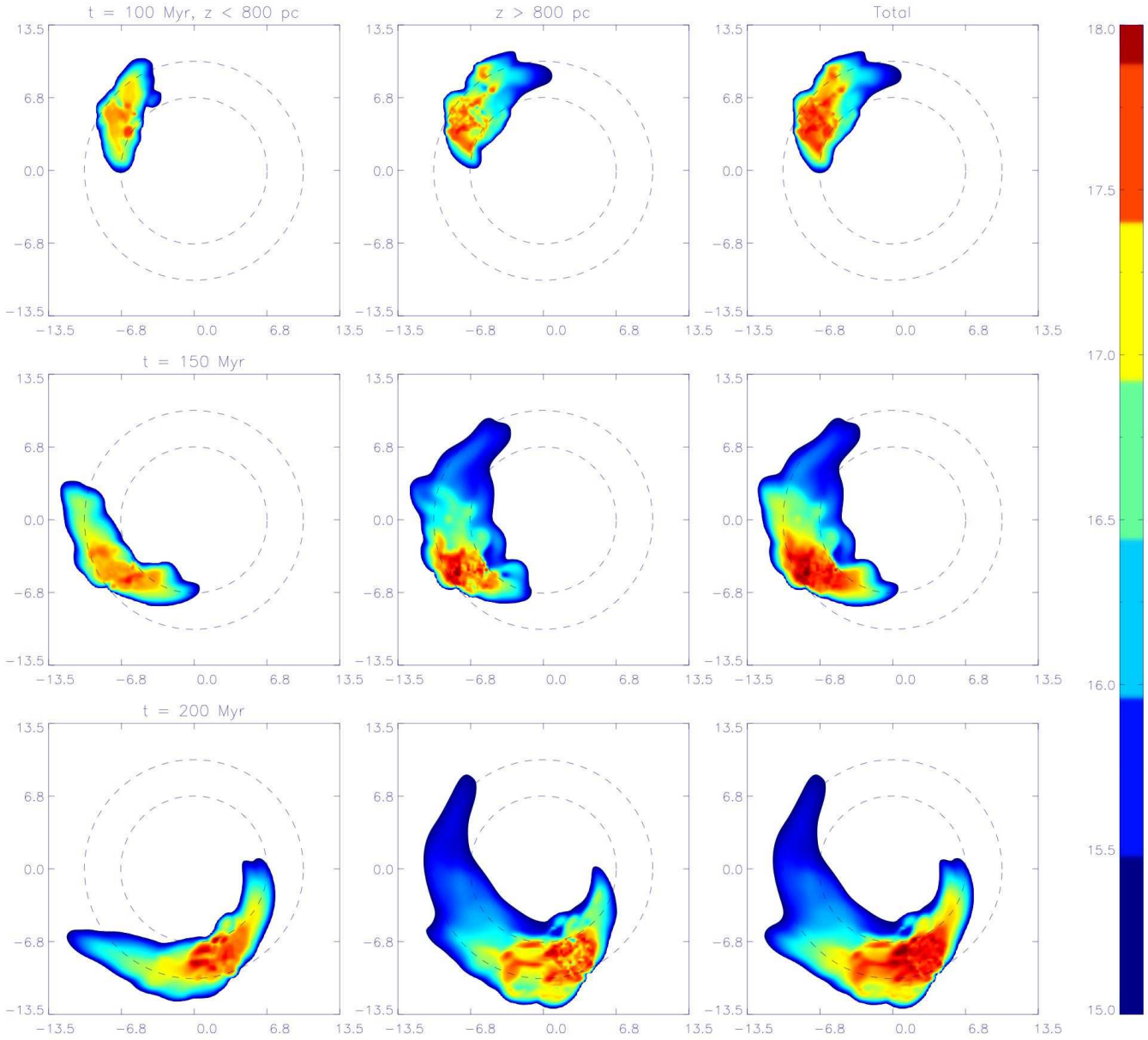

Figure 3. Column density along the z direction of the SN II ejecta for the reference model. Each row corresponds to a different time. The left and central panels correspond to the column densities calculated in the intervals $z < 0.8$ kpc and $z > 0.8$ kpc, respectively, where $z = 0.8$ kpc corresponds to the location of the disk/halo transition. The right column shows the total column densities. The two circles have the same meaning as in Fig. 2. The logarithmic column density scale is given in cm^{-2} and the spatial scale along the x and y directions is in kpc.

indicates that there is no substantial radial dispersal of the metals from the Galactocentric radius where they are produced. A similar result has been also recently reported by Spitoni et al. (2008).

Moreover, Figures 3 and 4 show that the small fraction of the rising gas escaping to the coronal sector moves radially preferentially outward rather than inward. This is due to the decrease of the centripetal component of the gravity with height and to the conservation of the angular momentum (Shapiro & Field 1976; Bregman 1980). The tendency of the MGF gas to move outward is however, contrasted by its interaction with the hot halo (which is assumed at rest). The fountain transfers part of its angular momentum to the halo and thus tends to reduce its radial displacement outward (see below).

A more quantitative insight of the evolution of the gas circulation is given by Fig. 5. The top panel shows the loss of angular momentum of the SN II ejecta due to the interaction with the halo gas [2]. At any time, the angular momentum displayed in the figure is normalized to the total

[2] We point out that the time evolution of the relative angular momentum of *all* the gas lifted by the fountains is quite similar to that relative to the SN II ejecta alone.

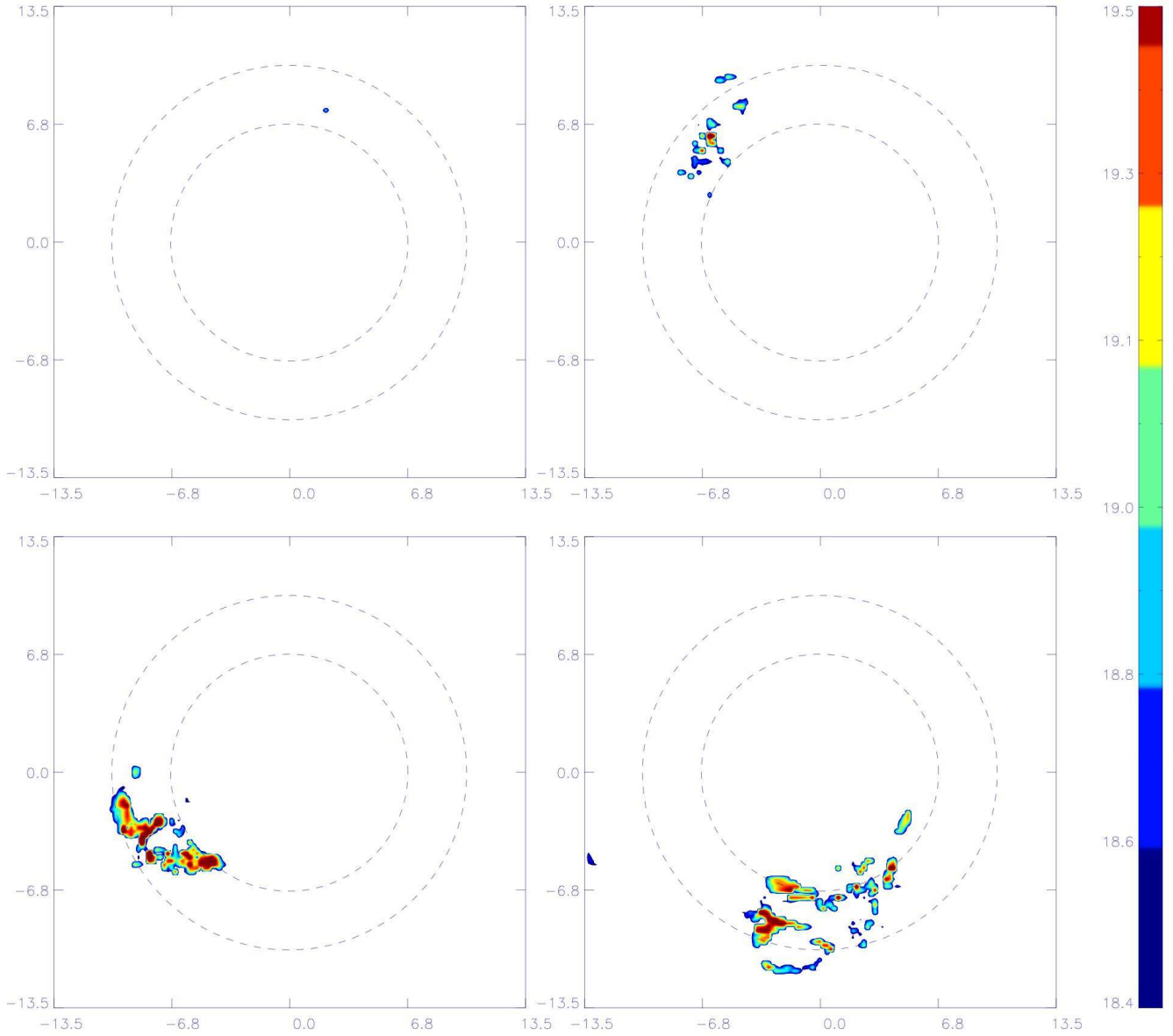

Figure 4. Column density along the z direction of the gas falling back to the disk, for the reference model. The times are the same as in Fig. 2, as well as the meaning of the two circles. As apparent from the figure, we consider only gas condensed into clouds and filaments. It is also clear that the clouds remain essentially within the circular sector in which the active area is located. The logarithmic column density scale is given in cm^{-2} and the spatial scale along the x and y directions is in kpc.

angular momentum injected by the SN II up to that time. The middle panel illustrates the fraction of the SN II ejecta located at different heights, while the bottom panel shows the fraction of ejecta moving outside of the boundary of the active area and testifies that the amount of gas moving outward is larger than that moving inward. The latter starts to increase after $\sim$ 70 Myr, when a substantial amount of the lifted gas starts to fall back (see section 3.4); having lost part of its angular momentum, this gas tends to return at a Galacocentric radius smaller than that at which it started its journey.

It is interesting to compare Fig. 5 with the analogous figure in Paper I (Fig. 5) in order to highlight similarities and differences with the SGF case. The relative loss of the angular momentum of the fountain gas is essentially the same. This must be expected as in MGFs a larger amount of fountain gas interacts with a larger amount of halo gas, leaving the loss of specific angular momentum essentially unaffected compared to SGFs. For analogous reasons, also the relative amount of gas lifted above different heights is similar; a larger amount of energy, in fact, moves a larger amount of gas to similar altitudes. Obviously, as the SN explosions keep going for a longer time, new gas persists at larger heights, at variance with the SGF case. Finally, we stress that in the case of SGFs on the long term the fraction of gas moving outward is smaller than that moving inward, at variance with the MGF case. However, a glance to Fig. 5 of Paper I reveals that, initially, also in the SGF case more gas moves

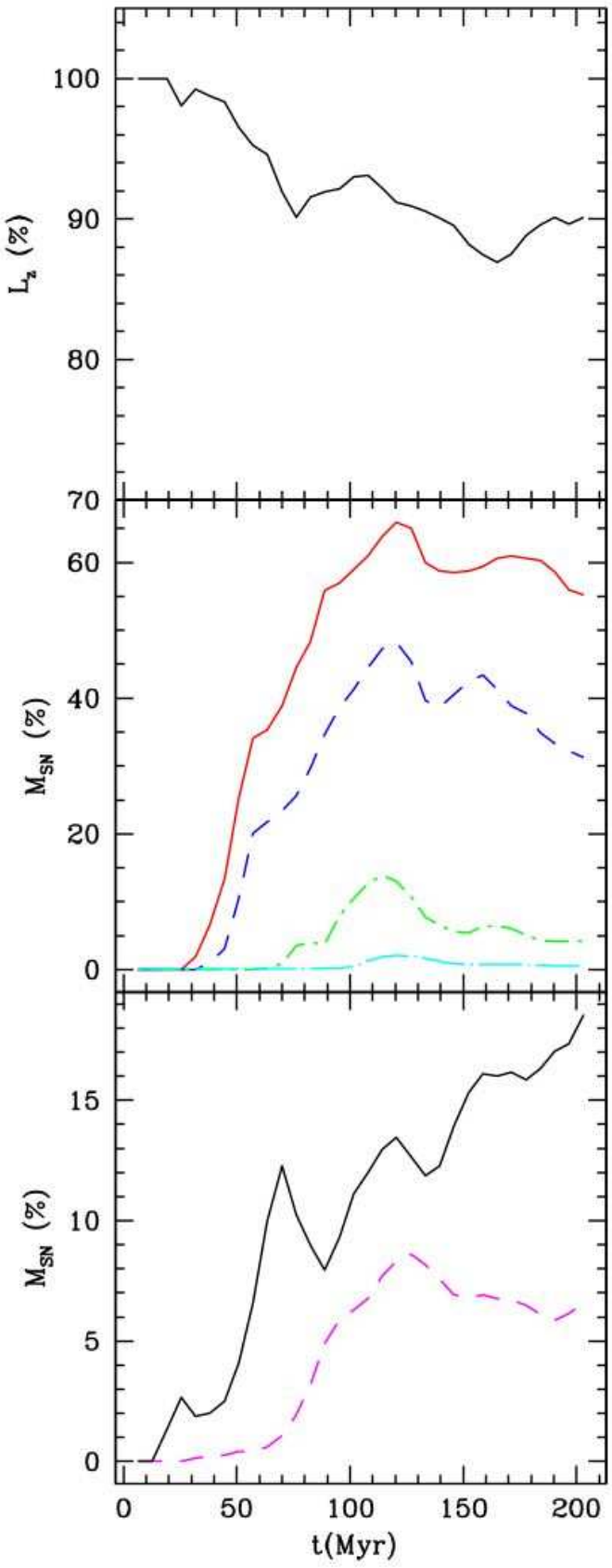

Figure 5. Illustration of several quantities for the reference model. Top panel: angular momentum evolution of the SNII ejecta normalized to the angular momentum injected by the SN II ejecta. Middle panel: fraction of the mass of SN II ejecta located at

outward rather than inward. This different behaviour is due to the fact that in the present model the MGF flow is continuously supplied, while in the SGFs the SN engine stops its activity after 30 Myr and the fountain gas, being no more replenished with fresh angular momentum, is facilitated in its centripetal displacement.

In any case, it is quite clear that most of the gas remains essentially at the same Galactocentric distance where it has been created.

3.3 Cloud properties

We now discuss in more detail the structure of the clouds forming from the gas powered by the MGFs. In particular, the ISM lifted by the fountains condenses essentially at the top of its trajectory, and than falls back with velocities $\lesssim 100$ km s^{-1}. ~ 130 Myr after the beginning of the simulation an equilibrium is established between ascending and descending gas (cf. sect. 3.4). After this time, the gas lifted above 1 kpc has a mass 1.5×10^7 M$_\odot$, 75% of which is condensed in dense filaments cooled down to $T = 10^4$ K (see Fig. 6). The clouds are composed essentially of gas originally from the disk ($\sim$96%), and only a slight contribution (4%) from the halo gas that was compressed and cooled after interacting with the fountains. As we have found in Paper I, the SN ejecta plays a negligible role in the mass budget of the fountains. After 130 Myr, 1.3×10^4 SNe II have exploded and delivered 2.1×10^5 M$_\odot$ of ejecta, but only half of it enters within the computational domain (the rest is injected in the "lower" half of the halo, which was not considered in our simulations, for symmetry reasons, as remarked in Sec. 2). Nearly 50% of the ejecta remains trapped within the disk, 35% is encompassed within the evolving clouds, and 15% floats over the disk as hot, diffuse gas. Thus the SN ejecta contribute for less than 0.4% to the clouds mass. For this reason, the chemical composition of the clouds is unaffected by the metals produced by the SNe II driving the fountains. As each supernova delivers on average 3 M$_\odot$ of metals (cf. Marcolini et al. 2007), a total mass of 2×10^4 M$_\odot$ of heavy elements is ejected by the fountain within the computational domain. As a result, the metallicity increment in the clouds due to the freshly delivered metals is $\Delta Z = 5.7 \times 10^{-4}$, rather negligible compared to the solar metallicity of the ISM. This conclusion holds also if one considers the contribution of SNe II belonging to OB associations hosting less than 30 SN progenitors, and representing half of the total number of supernovae (see section 2.2.2).

In conclusion, the clouds forming in our simulation have solar metallicities and velocities lower than 100 km s^{-1}, and are therefore likely to be associated to IVCs rather than HVCs (Wakker et al. 2008). This result is in agreement with that found in Paper I when considering single fountains.

3.4 Disk-halo energy exchange

Other details of the gas flows of the reference model are given in Fig. 7, and are intended to shed light on the feedback between the disk and the hot halo. This energy exchange regulates the evolution of the halo gas and influences the star formation history in the disk. It is also relevant in the related issue of the so-called "over-cooling" problem in cosmological simulations of galaxy formation, which generally

overestimate the amount of radiatively cooled gas in galaxies. Energy feedback from SNe and/or AGN, albeit poorly understood, is thought to be a crucial ingredient to reconcile hierarchical models of galaxy formation with the observations (e.g. Navarro & Steinmetz 1997; Croton et al. 2006). Supernovae alone are probably incapable to fully solve the problem (Tornatore et al. 2004), but is nevertheless important to quantify the SN energy which heats the hot halo gas to correctly estimate its cooling rate and the disk-halo mass exchange.

As in our model the amount of thermal energy of all the halo is much larger than the energy injected by the SNe, a direct evaluation of its variation due to the stellar explosions would be rather inaccurate (also because of the perturbations generated at the grid boundaries, as discussed in Paper I). We thereby check the energy balance of the halo-fountains interaction as follows. In the top panel of Fig. 7 we report the thermal energy of the disk gas that is lifted by the fountains and not condensed into clouds. This rarefied gas endures over the disk and its thermal energy is incorporated in the hot halo. On the other hand, some coronal gas cools and condenses over the clouds created by the MGFs. The thermal energy radiated by this cold gas is also shown in the top panel of Fig. 7. At the end of the simulation, the halo has gained an energy twice larger than that radiated due to the interaction with the fountains, with a net increase of thermal energy of $\sim 10\%$ of the energy released by all the SNe. This value for the SNe heating efficiency is expected to remain stable once an approximately steady regime is established between rising and falling gas.

The achievement of this regime is visible in the middle panel of Fig. 7 that shows the fraction of rising (solid line) and descending (dashed line) fountain gas. At early times only the rising gas is present. After nearly 40 Myr the first clouds form and fall back. A dynamical equilibrium between ascending and descending gas is established after 130 Myr. The same result is illustrated in the bottom panel in terms of the absolute values of the rising and falling masses.

As pointed out, we cannot make an exact evaluation of the energy balance between the fountains and the coronal gas. In the analysis above (see the top panel of Fig. 7), we neglected the gain of the kinetic energy of the hot gas interacting with the galactic fountains and the change in the potential energy of the whole halo. Also, we neglected the radiative losses of the hot gas, possibly enhanced by the compression due to the fountain expansion. However, the flow of the halo gas remains subsonic and its cooling time is longer than the time of the simulation. We thus conclude that a net energy gain is attained by the halo during its interaction with the MGFs.

4 MODEL AT R=4.5 KPC

In this section we explore the influence of the Galactocentric distance on the gasdynamics of the MGFs. In particular, we have run a model similar to the RM, but with the active area centred at $R = 4.5$ kpc. Here the gas of the disk is denser and has a larger effective vertical scale heigh $H_{\rm eff}$. As a consequence, the disk-halo transition occurs at $z = 1.35$ kpc, instead of $z = 0.8$ kpc as in the RM (see also Paper I).

The larger density of the ambient medium makes more

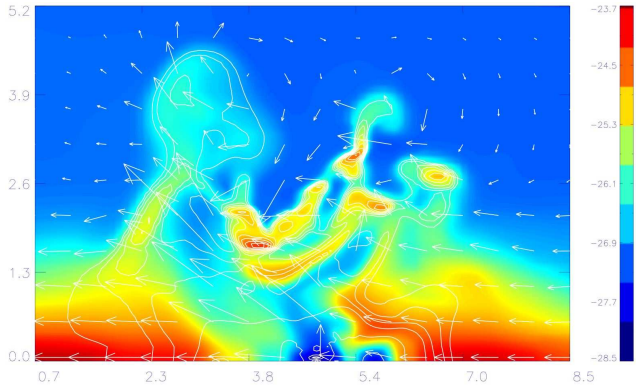

Figure 6. Distribution of the disk gas at $t = 130$ Myr at the plane orthogonal to the Galactic disk and passing through the active area for the reference model. Isodensity curves of the ejecta are over-imposed, highlighting the fountain pattern and the cloud formation. Since the density of the ejecta is much smaller than that of the ISM, it is represented in a different scale in order to be visible in the figure. The logarithmic density scale of the disk gas is given in g cm^{-3} and the spatial scale along the x and z directions is in kpc.

difficult the expansion of the SN bubbles through the plane and accelerates their backfilling. The reduced size and lifetime of the holes also reduce their probability of merging. This is apparent in Fig. 8, where the number and the size of the holes are smaller than in the reference model (cf. Fig. 2).

In Paper I it was shown how the vertical distribution of the disk gas influences the dynamics of a SGF and the shape of the chimney carved by the fountain. In particular, a single fountain located at $R = 4.5$ kpc gives rise to a sort of well collimated outflow that crosses the disk/halo transition only barely. On the contrary, given the lower density and scale height of the local gas, the same fountain located at $R = 8.5$ kpc experiences a well defined break out. In the case of MGFs these differences are greatly reduced because the energy powering the gas flow in this case is much larger than the critical luminosity $L_{\rm cr}$ at any Galactocentric distance.

A somewhat larger alignment is still present at $R = 4.5$ kpc also in the case of MGFs, as apparent when one compares Fig. 3 with Fig. 9 (where the different position of the disk/halo transition has been taken into account). The amount of diffuse gas spread outside the circular sector is smaller than in the RM. The same conclusion can be reached looking at Fig. 10. The falling gas is clearly less radially dispersed compared to the reference model (cf. Fig. 4). Note that, since in the present model the circumference covered by the active area is shorter, after 200 Myr a complete ring is described in all the panels of the bottom raw of Fig. 10.

As for the RM, more quantitative information can be obtained looking at the Fig. 11. The loss of angular momentum is essentially the same as in the RM (top panel). Comparing to the SGF evolution (Fig. 9 in Paper I), we remark that in this latter case the angular momentum, after an initial drop, slowly goes up again. As discussed in Paper I, this is due to the fact that a larger fraction of the SGF gas falls back onto the thicker disk gaining new angular momentum. This effect is not present in the MGF model because,

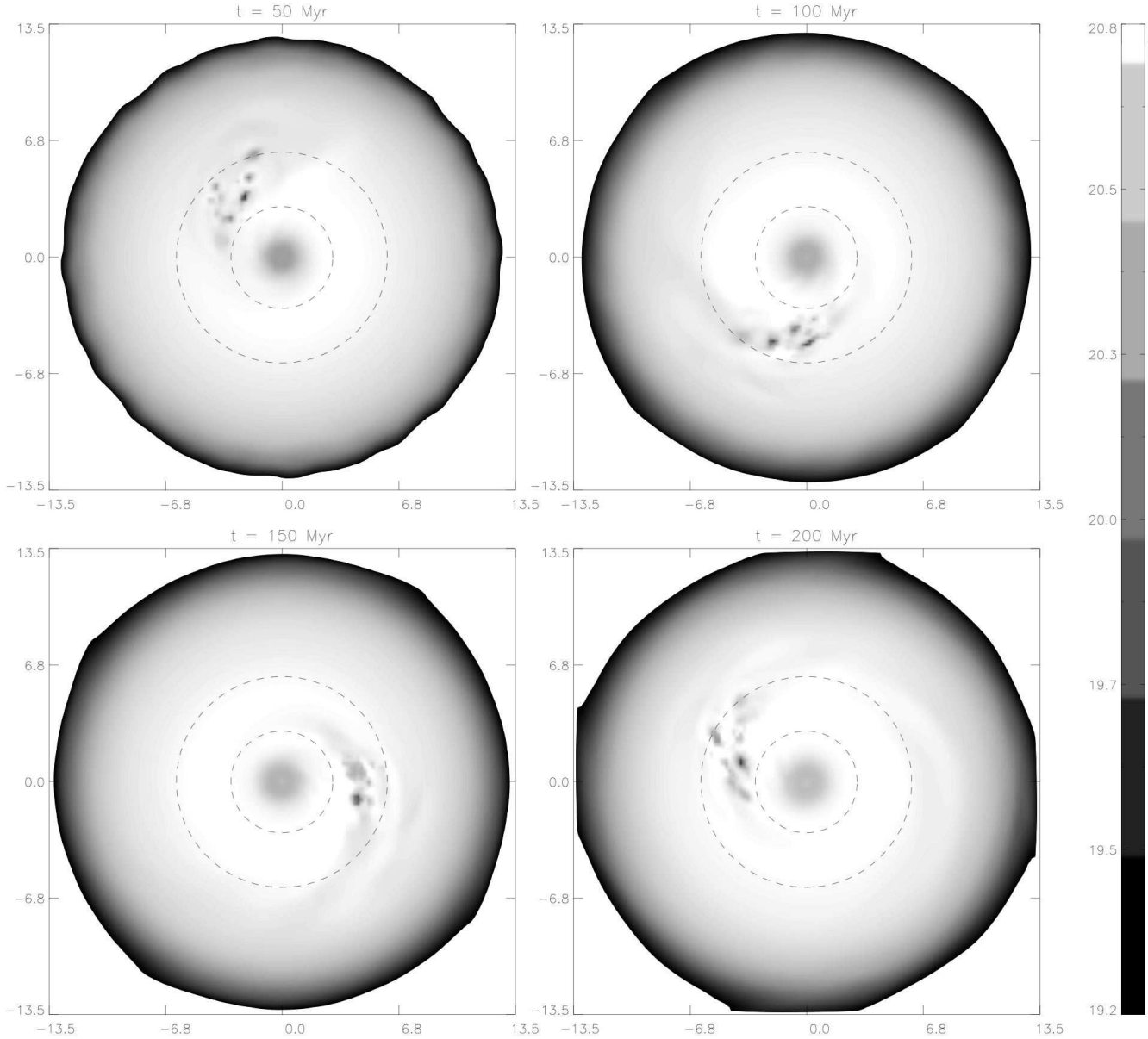

Figure 8. The same as in Fig. 2, but for the Galactocentric distance $R = 4.5$ kpc.

as stressed above, given the larger energy of the fountain, the disk thickness does not play a significant role

The vertical extent covered by the gas (middle panel of Fig. 11) is somewhat lower than in the RM as the density and the scale height of the disk are larger in this case. The differences with the SGF case are analogous to those discussed for the RM, and do not repeat them here.

The smaller radial dispersion of the MGF gas emphasized above is illustrated in the bottom panel of Fig. 11 showing that the amount of gas moving radially outside the active area in nearly halved compared to the RM.

Finally, from the top panel of Fig. 12 we see that in this model the halo gas acquires 10% of the SN energy at the end of the simulation, i.e., the same amount as in the RM. Also the time at which the quantity of ascending and descending gas become comparable is similar to that of the RM (middle and bottom panels of Fig. 12).

5 INTERACTION WITH ACCRETING GAS

As pointed out in Sec. 1, the gas flow of the fountains is likely to sweep up cold gas, but it is unclear whether this gas arises from cooling of the hot halo or from cold streams falling from large distances. Fraternali & Binney (2008) argue that this latter possibility is the most realistic. If the cold falling gas is clumpy, its clouds cannot be more massive than 10^7 $M_\odot$, otherwise the solar neighbourhood would be heated by their passage (Lacey & Ostriker 1985; Toth & Ostriker 1992). Actually, while HVCs surrounding our Galaxy have masses of order 10^{6-7} $M_\odot$ (e.g. Wakker et al. 2008), deep

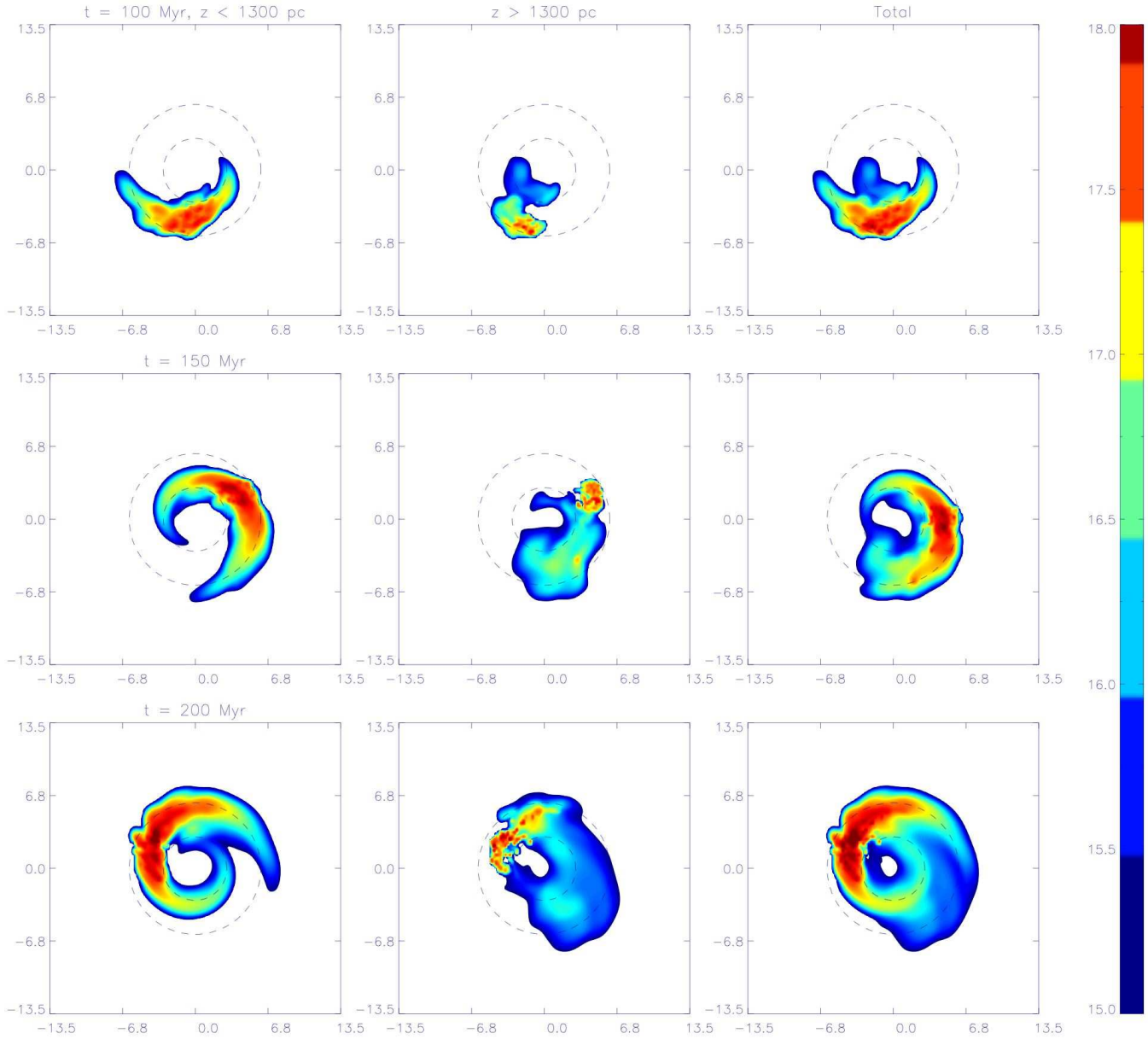

Figure 9. The same as in Fig. 3, but for the Galactocentric distance $R = 4.5$ kpc. In this case the left and central panels give the column densities calculated in the intervals $z < 1.3$ kpc and $z > 1.3$ kpc, respectively, since at this Galactocentric distance the disk/halo transition occurs at $z = 1.3$ kpc.

observations around M31 reveal the presence of numerous HVCs with masses down to 10^4 $M_\odot$ (Westmeier et al. 2005).

The study of the possible accretion of gas onto galaxies is important for several reasons. It is generally believed that accretion must replace the gas consumed by star formation which has been remarkably constant in the solar neighbourhood over the Galaxy lifetime (e.g. Binney et al. 2000). Another reason for studying the galactic accretion is linked to the mounting evidence of massive haloes of neutral and ionized gas surrounding nearby spiral galaxies (e.g. Sancisi et al. 2008). These thick disks rotate more slowly than the thin disks and show inflow motions. Fraternali & Binney (2008) have shown that these haloes cannot be sustained only by galactic fountains. According to them, the gas from the fountains interacting with a pre-existing hot corona would make it to co-rotate with the disk after a very short time ($\lesssim 1$ Myr) which is not consistent with the observations. This result led them to conclude that a substantial accretion of low angular momentum material from the intergalactic medium would be required in order to assure a slower rotating halo.

In the model of Fraternali & Binney (2008) the clouds are treated as bullets moving ballistically, and hydrodynamical effects are absent or only roughly represented. In order to investigate the issues above more realistically from an hydrodynamical point of view, we have simulated the interaction of the MGFs with infalling gas considering two different models, one in which the gas infall is described as

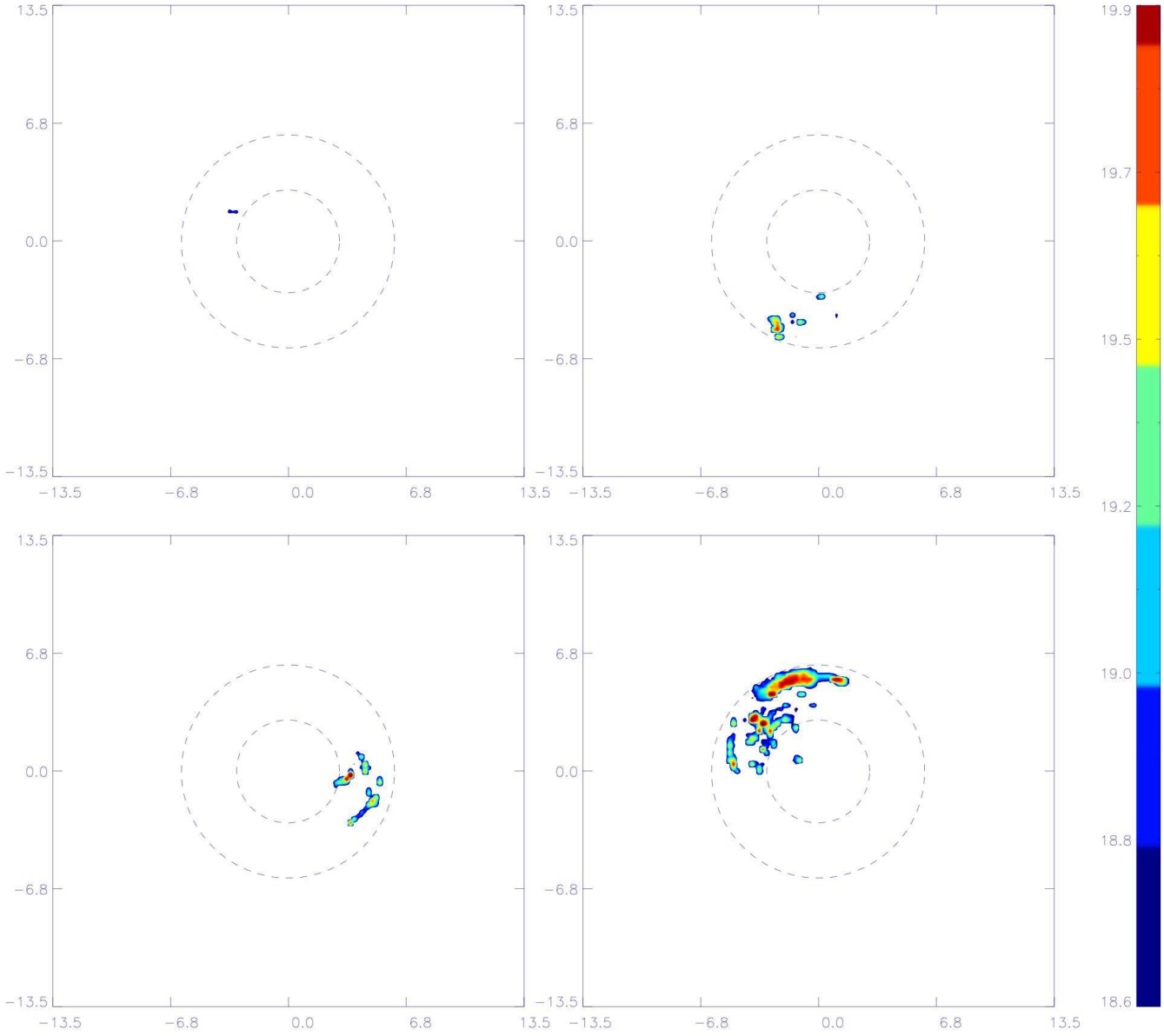

Figure 10. The same as in Fig. 4, but for the galactocentric distance $R = 4.5$ kpc

a continuous drizzle, and another in which a single, denser cloud is assumed to fall toward the active area.

5.1 The "drizzle" model

This model is similar to the reference model, but we assume that a gas of density $n = 10^{-3}$ cm^{-3} drops from the "top" boundary of the computational grid with a vertical velocity $v_z = -150$ km s^{-1}. Such a flux extended over all the Galactic disk would correspond to an accretion rate of 5.2 M$_\odot$ yr^{-1} (from both sides). This is much higher than the accretion rate $\dot{M} \sim 0.2$ M$_\odot$ yr^{-1} associated with the HVCs, and also higher than the rate of ~ 2 M$_\odot$ yr^{-1} needed to sustain the star formation in the solar neighbourhood. However, the accretion rate we assume is comparable to that in Fraternali & Binney (2008) (which was adopted for the case of NGC 891) and this will allow a direct comparison with their work.

As we consider the fountain activity only in a limited region of the disk plane, we let the rain fall from the top boundary only over the ring sector on the disk where the active area moves (cf. Fig. 2). We have considered only this region because most of the gas set in motion by the fountains remains within this sector (as we have seen in section 3), so that all the features of the interaction of the fountains with the rain can be captured.

As the infalling gas interacts with the hot halo and with the ascending gas of the fountains, vortices of ~ 2.5 kpc form and the density of the gas above the disk fluctuates, as shown in Fig. 13. These vortices are likely an artifact of the method we use to inject the accreting gas. However, these features do not alter the flow generated by the fountains, being the vortices energetically negligible compared to the

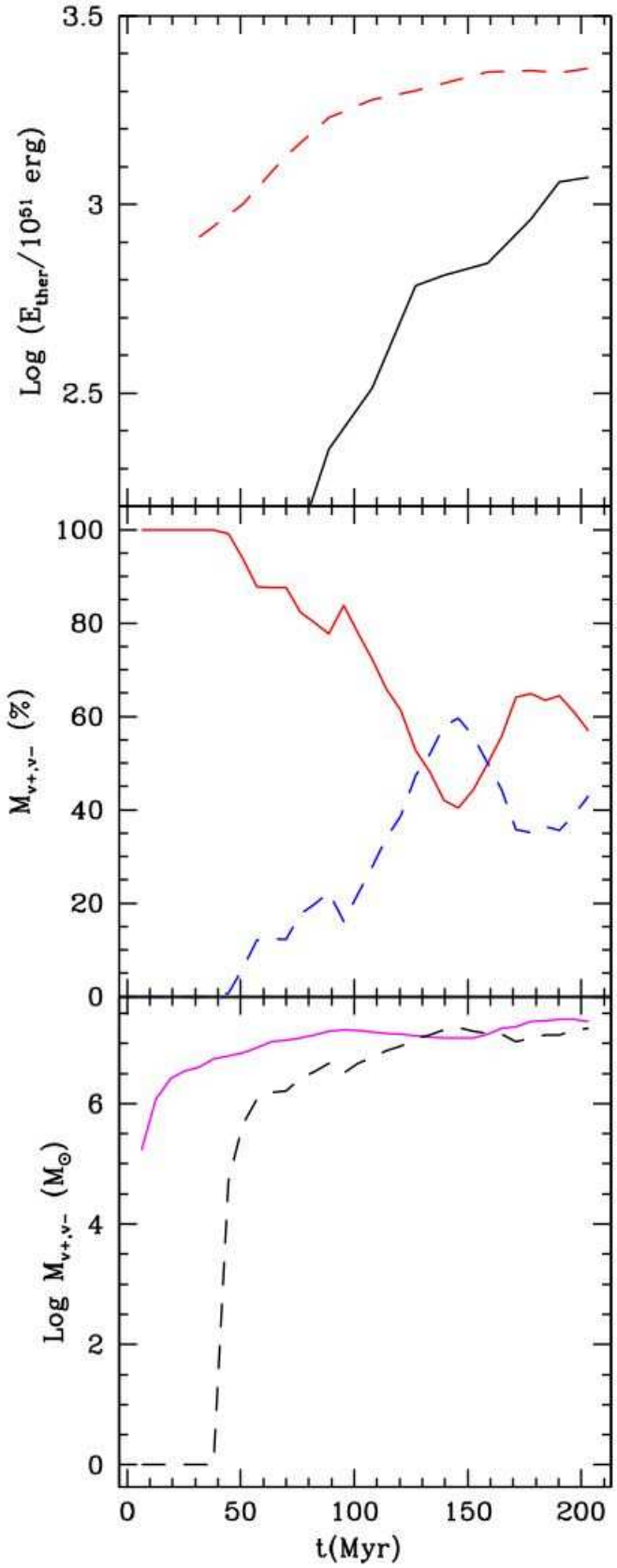

Figure 7. Illustration of several quantities of the reference model. Top panel: amount of thermal energy of the disk gas transferred to the gaseous halo (solid line), thermal energy lost by the halo gas condensed onto the clouds (dashed line); see text for details. Middle panel: fraction of the total amount of gas that is rising

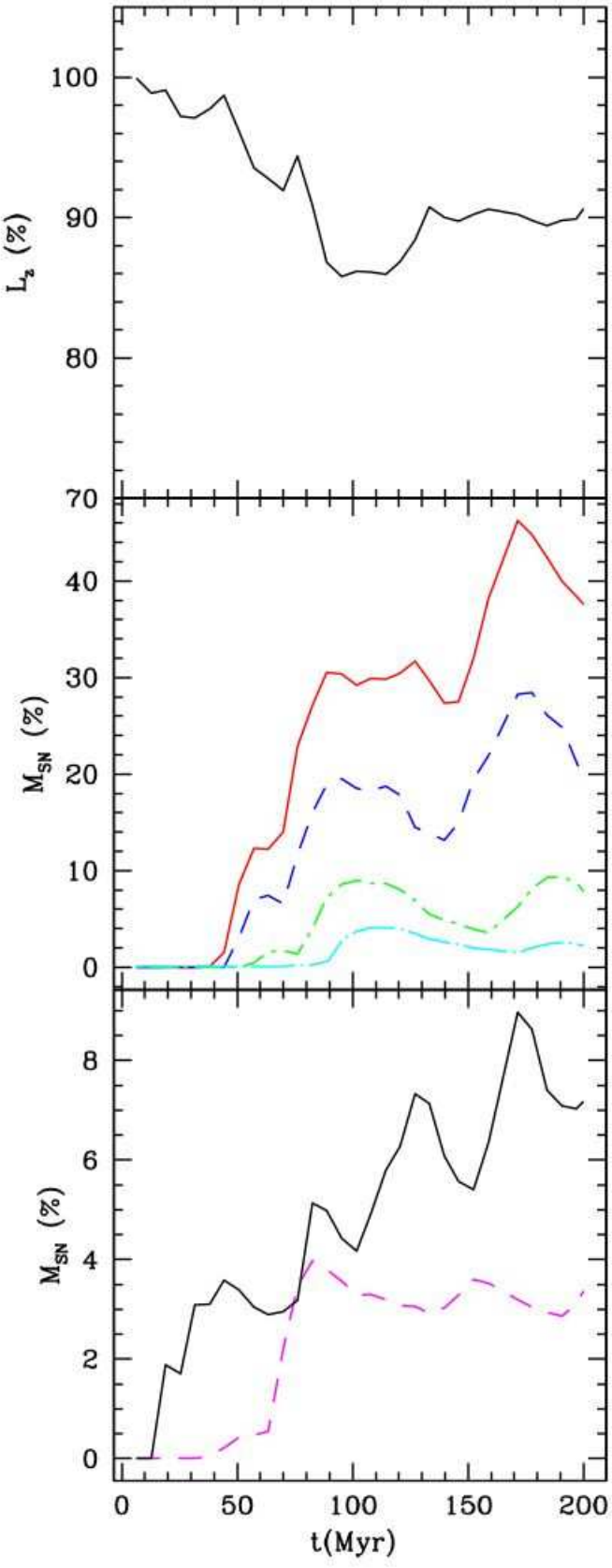

Figure 11. The same as in Fig. 5, but for the model with the active area centred at the Galactocentric radius $R = 4.5$ kpc.

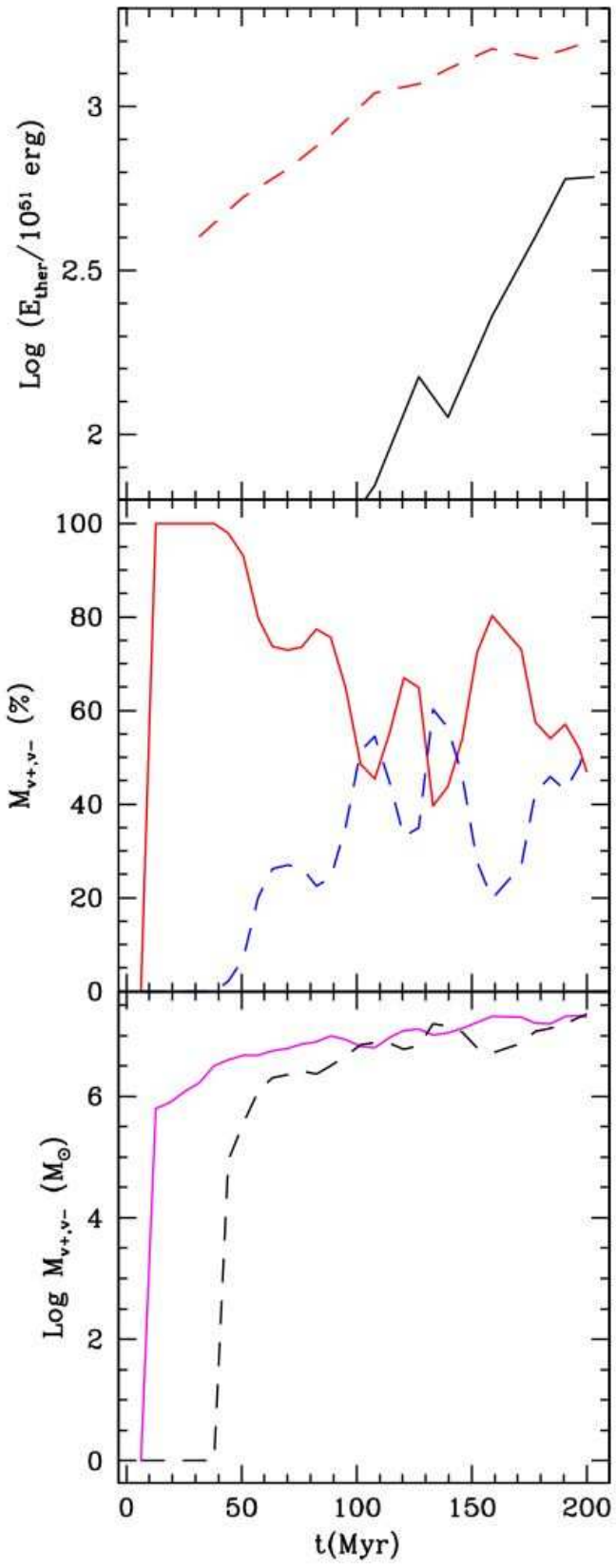

Figure 12. the same as in Fig. 7, but for the model with the active area centred at the Galactocentric radius $R = 4$ kpc.

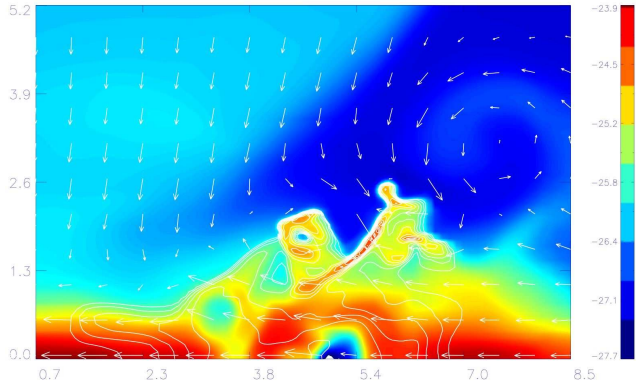

Figure 13. The same as in Fig. 6, but for a model considering a continuous external gas infall over the active area (the drizzle model).

energy injected by the SNe. Figure 13 corresponds to the same time and grid slice of the snapshot depicted in the RM of Fig. 6. Comparing both models, we see that in the drizzle model the disk gas set in motion by the fountains reaches lower heights and tends to lag behind the active area (toward the right hand side in the figure).

A more quantitative analysis is given in Fig. 14. The angular momentum loss (top panel) is more than doubled relative to the RM. This explains the larger lag of the fountain flow relative to the disk, as noted above. The middle panel quantifies the vertical distribution of the fountain gas; it is essentially similar to the reference model up to $z = 1.2$ kpc (cf. Fig. 5), but less gas is found above $z = 2.4$ kpc.

Once an overall balance is reached between ascending and descending gas, as in the RM, 25% of the lifted gas remains rather diffuse, while 75% of it condenses in dense filaments. The total mass of these clouds is 7×10^6 $M_\odot$, i.e., nearly 60% of what was found in the RM; such reduction is related to the lower vertical excursion of the clouds and their shorter "lifetime". It is interesting to analyze the "composition" of the clouds. As in the RM, the contribution to their mass by the SN ejecta amounts to a negligible 0.3%. This time, however, the amount of disk gas is lower (87.9%), while the fraction of "external" gas is three times larger (11.8%). This result is obviously due to the addition of the rain material to the halo gas. This denser ambient medium cools more easily when it interacts with the clouds and condenses onto them more efficiently.

The accretion mass onto the clouds is a crucial ingredient in the model of Fraternali & Binney (2008). In their model, they integrated the orbits of the clouds that are ejected from the disk of a spiral galaxy and move up ballistically to the halo and then return to the disk. As the clouds accrete mass from external infalling gas, their velocity decreases due to momentum conservation. These authors have then shown that, if the thick disk of neutral gas of the spiral galaxies is made up of clouds lifted by galactic fountains, the accretion of external gas with low angular momentum could explain why the observed rotational curve of these disk galaxies decreases with z. It is interesting to compare our results with those found by Fraternali & Binney (2008).

In order to evaluate the mass accretion onto our clouds, let us define m_0 as the "initial mass of the clouds" (i.e., the

mass of the disk gas lifted by the fountains that has condensed into clouds), and δm as the amount of ambient gas (i.e. the gas of the halo and the drizzle) that is swept by the clouds and increase their mass up to $m = m_0 \delta m$. From our simulations, we obtain $\delta m/m_0 = 0.13$; this result is in reasonable agreement with what found by Fraternali & Binney (2008) in the case of NGC 2403 (cf. their Fig. 6).

We can pursuit further the analysis above computing the specific accretion rate $\alpha = \dot{m}/m$. To this end we must evaluate the clouds' lifetime $t_{\rm lf}$ in order to work out $\alpha = \delta m/(m_0 t_{\rm lf})$. From Fig. 15 we note that ascending and descending gas reach a dynamical equilibrium after $t \gtrsim 70$ Myr. This is thus the characteristic time spent by a cloud during its journey, we obtain $\alpha \sim 1.9$ Gyr^{-1}, which is in good agreement with the value $\alpha \sim 2$ Gyr^{-1} found by Fraternali & Binney (2008). Although this agreement must not be super-estimated given the approximations involved in the previous calculations, yet we consider it significant.

We now evaluate how the external mass accretion onto the clouds affects their rotational velocity. Obviously, given the limited extension of the active area in our model, we cannot build a thick disk of neutral hydrogen out of it, nor reproduce the entire disk rotational curve. However, some interesting conclusions can be drawn from the simulations above. The time evolution of the rotational velocities at $z = 1.8$ kpc are illustrated in the top panel of Fig. 16 for both the reference and the drizzle models. They give the mass weighed mean velocity of a "slice" of clouds at $z = 1.8$ kpc. Likewise the angular momentum (cf. the top panels of Figs. 5 and 14), the values of the velocities tend to stabilize after an initial drop.

It is an easy matter to verify whether the difference in the cloud rotation velocity between the drizzle model and the RM is entirely due to the difference in the amount of mass increment (as suggested by the ballistic model of Fraternalli & Binney 2008), or not. In that case we would have

$$\frac{v'_{\rm rot}}{v_{\rm rot}} = \frac{1 + \frac{\delta m}{m_0}}{1 + \frac{\delta m'}{m'_0}}, \qquad (4)$$

where the prime quantities refer to the drizzle model. From Fig. 16 we find that at $t = 200$ Myr, $v'_{\rm rot}/v_{\rm rot} = 0.83$. On the other hand, computing the amount of accreted matter onto the clouds from the simulations we find that the right hand side of equation (4) gives a larger ratio $v'_{\rm rot}/v_{\rm rot} = 0.92$. This means that only part of the rotation velocity drop is due to the accretion of external material to the clouds. A rough estimate of the total momentum flux of the system (that includes both the clouds momentum flux and the halo gas and ram pressures) indicates that the remaining drop of the rotation velocity of the clouds is due to their interaction with the hot halo which in the case of the drizzle model is much denser due to the external accretion.

In conclusion, though our simulations are restricted to a small area of the Galactic disk, and therefore are not suitable to reproduce the rotational curve of the entire thick disk or of the hot halo, they seem to indicate that the presence of an external gas infall may help to slow down the rotation of the gas in the clouds (see Fig. 16) and thus the amount of angular momentum that is transferred to the coronal gas, as suggested by Fraternali & Binney (2008).

A final remark is in order with regard to the discussion above. In the model of Fraternali & Binney (2008) the clouds are described as pellets that preserve their identity during all their journey until the return to the disk. Let us define χ as the ratio between the density of the cloud and that of the hot halo, and the flow time as $t_{\rm flow} = D/v$, where D and v are the cloud diameter and velocity, respectively. Fraternali & Binney (2008) estimate that typically $\chi \sim 300$, $D = 100$ pc and $v = 100$ km s^{-1}. With these figures, it turns out that the orbital time of a cloud is of the same order of the drag time $t_{\rm drag} = \chi t_{\rm flow} \sim 300$ Myr. However, a cloud can be destroyed by Kelvin-Helmholtz (K-H) instabilities in a time scale $t_{\rm KH} = \chi^{0.5} t_{\rm flow} \sim 17$ Myr. Thus, in the model of Fraternali & Binney (2008) the cloud material is likely to linger above the disk as diluted gas. In our models, instead, the clouds never reach very large densities, and for the densest structures we obtain $\chi \sim 100$ and $D \sim 500$ pc. As a consequence, it is $t_{\rm KH} \sim 50$ Myr, which is of the same order of the cloud lifetime. Simulations with higher spatial resolution would be required in order to follow appropriately how the cloud evolution is influenced by K-H instabilities. Such more demanding simulations are planned in a near future.

5.2 The "cloud" model

In this section we study the effect of an external cloud falling toward the galaxy on the fountain gas dynamics. We do not follow the subsequent interaction between the cloud and the disk gas (see Bregman 2004, and references therein for a review on this subject). We consider a cloud entering the grid with a velocity $v_{\rm z} = -150$ km s^{-1} from the top boundary, with mass $M = 3.5 \times 10^6$ M$_\odot$, which is consistent with the estimate for Complex C (Miller et al. 2008). We also assume $T = 10^4$ K and density $n = 0.2$ cm^{-3}. The cloud is assumed to be initially cylindrically shaped with both diameter and height equal to 800 pc. Figure 17 shows a sequel of snapshots taken at different times and illustrating the dynamical interaction of the falling cloud with the rising gas of the MGF.

The figure shows that the cloud actually interacts only with a fraction of all the MGF gas. In fact, the cloud diameter is ~ 1.2 kpc (the cloud expands somewhat during its trajectory before entering in equilibrium with the ambient gas), and its covering factor relative to the active area is ~ 0.15. As a consequence, the general characteristics of the fountains are not greatly altered by the cloud interaction, as clearly illustrated in Fig. 18.

6 CONCLUSIONS

In Paper I we studied the evolution of a single fountain, i.e. the flow generated by a single SN II association, in order to understand the influence of a number of factors (such as the Galactic rotation, the distance from the centre of the Galaxy, and the presence of a hot Galactic halo) on the fountain gas circulation and on the properties of the clouds forming in this process. In the present paper, we have instead considered multiple GFs, i.e., the action (and interaction) of several GFs powered by SN II associations sufficiently close one to another in space and time. As in Paper I, we focused on a model located at $R = 8.4$ kpc, the solar Galactocentric distance. Our findings can be summarized as follows:

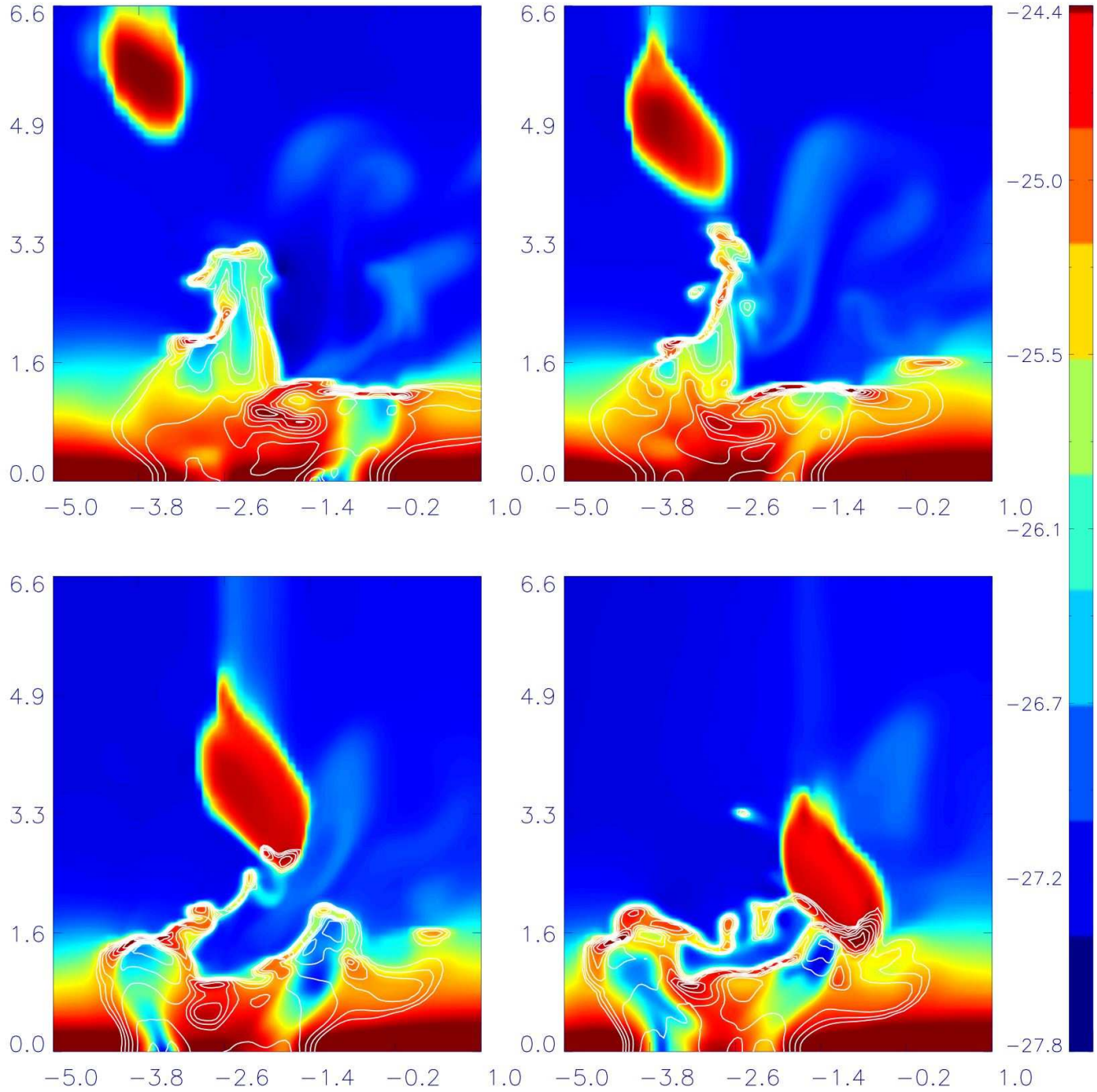

Figure 17. The same as in Fig. 6, but for the cloud model, where an external cloud falls over the MGFs. The four panels represent snapshots taken at $t = 130$ Myr (top-left), $t = 136.5$ Myr (top-right),$t = 143$ Myr (bottom-left),$t = 149.5$ Myr (bottom-right). As the Galaxy rotates, the falling cloud appears to move rightward.

(i) The spatial and temporal random sequel of SNe II produces holes on the disk, giving "punctured" look to it, qualitatively similar to what is observed in many galaxies, as NGC 2403 (Fraternali et al. 2002). The detailed "topology" of the gaseous disk depends on several factors such as the SN II rate, the size of the holes (which in turn depends on the clustering of the SNe and the local density of the ISM – See Section 4), and the speed at which they disappear once the SNe responsible of their formation stop exploding.

(ii) As expected, a larger amount of extraplanar gas can be found at larger heights relative to a SGF model. However, and somewhat more unexpectedly, the fountain flow remains radially localized, just as in the SGF case. The radial dispersion of the MGF gas, instead, is smaller than in the case of a SGF. Given the absence of significant radial flows, the fountains play a negligible role in shaping the radial profile of the disk chemical abundance, as required by chemical models which ignore the hydrodynamics of the ISM (e.g.,(Cescutti et al. 2007)).

(iii) Multiple fountains can form extraplanar gas at larger

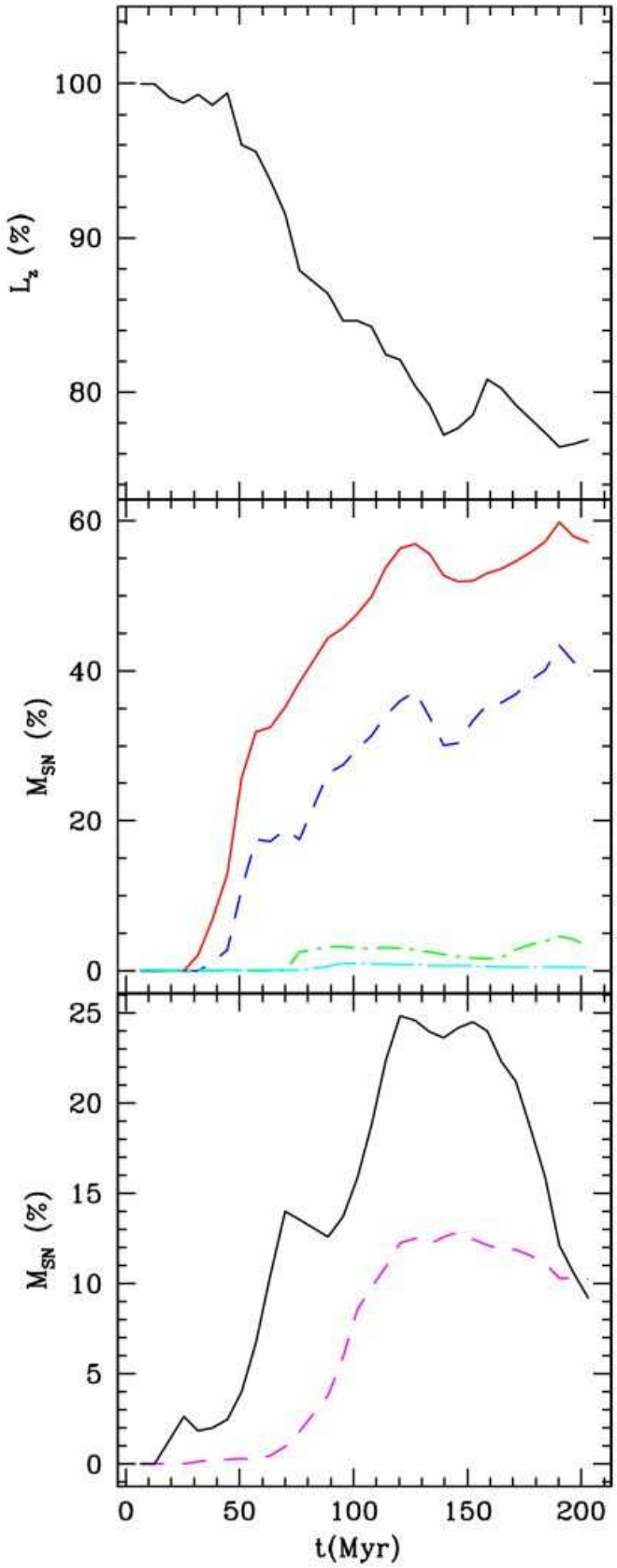

Figure 14. The same as in Fig. 5, but for the drizzle model.

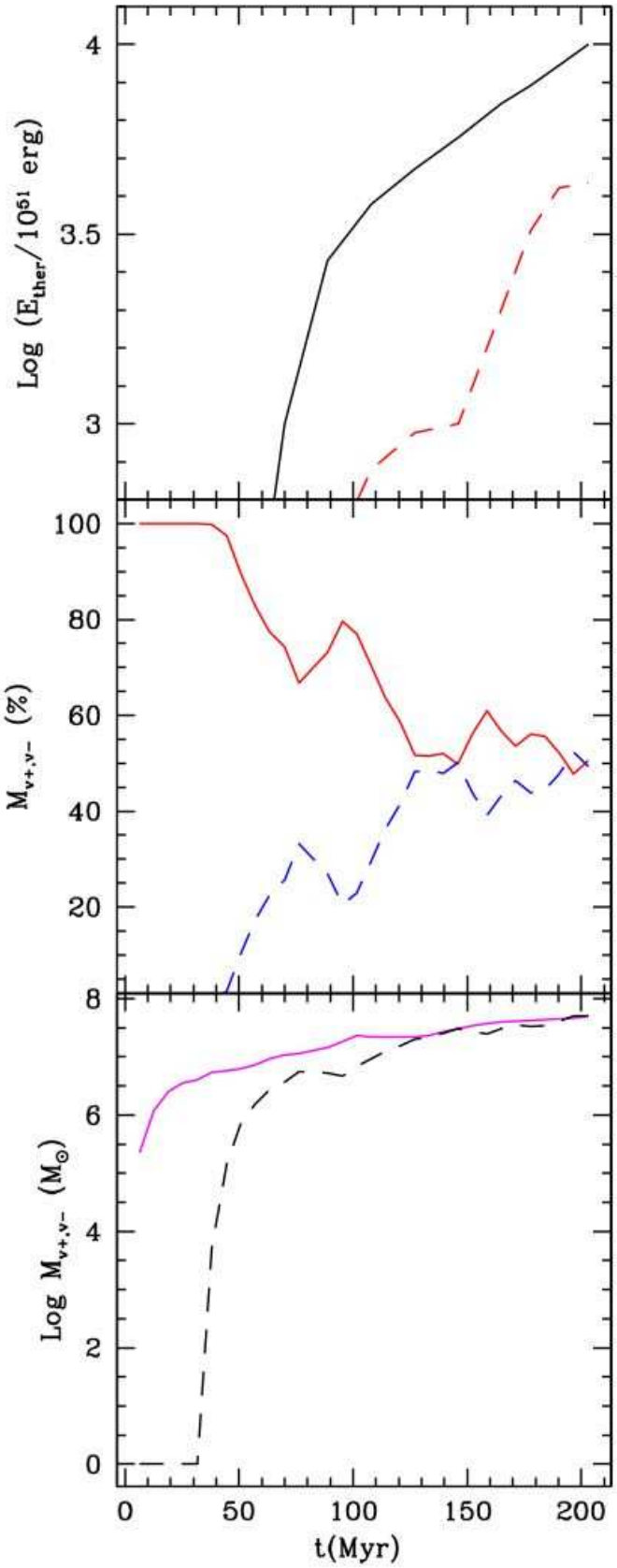

Figure 15. The same as in Fig. 7, but for the drizzle model.

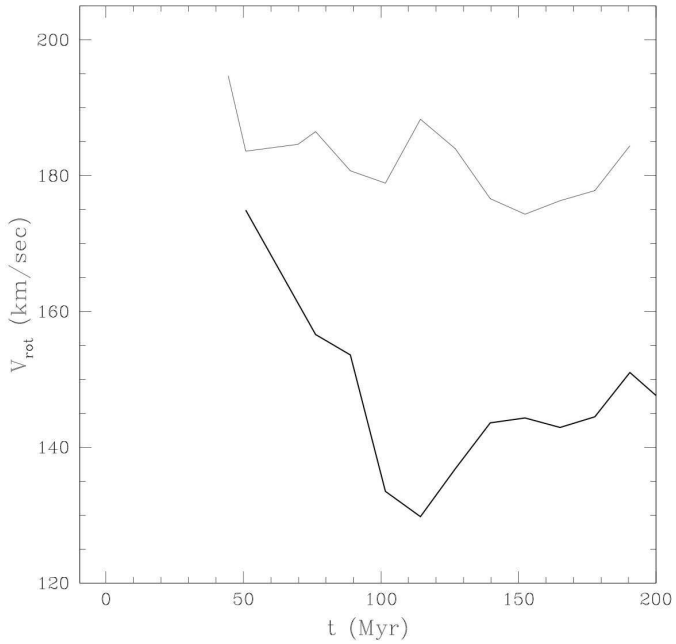

Figure 16. Time evolution of of the circular velocities of the clouds at $z = 1.8$ kpc for the reference model (thin line) and the drizzle model (thick line).

heights compared to SGFs. However, despite their higher energy budget, the MGFs are not able to produce clouds at an altitude larger than $\sim$ 3.5 kpc above the Galactic plane. Importantly, these clouds are mainly made of disk ISM (thus sharing the solar metallicity), rather than cooled SN ejecta or halo gas. They fall back toward the Galactic plane with velocities lower than 100 km $^{-1}$. From the considerations above we conclude that the gas condensations rising in our simulations can be identified with IVCs (rather than HVCs). In this scenario, the IVCs have a local origin (c.f. Wakker et al. 2008).

(iv) After the break out the multiple fountains protrude into the hot gas surrounding the Galaxy and an energy exchange is established between them and the hot gas. The diffuse fountain gas which does not participate of the cloud formation stays over the disk and becomes part of the halo gas. Its thermal energy remains in the hot halo. On the other hand, part of this coronal gas cools radiatively and condenses on the clouds. We find that the final balance is in favor of the halo, which is heated by the SNII with an efficiency of $\sim$ 10%. While this moderate value implies that SN feedback is probably not able to solve the "overcooling" problem that arises in the cosmological context of galaxy formation (e.g. Navarro & Steinmetz 1997; Tornatore et al. 2004) it is more that enough to mantain an extended hot gaseous halo and cold/warm extraplanar gas around typical spiral galaxies.

(v) Our hydrodynamical simulations indicate that the extraplanar gas generated by the fountains accretes mass from the infalling IGM at a rate similar to that inferred by Fraternali & Binney (2008). Though our simulations are restricted to a small area of the Galactic disk and therefore, are not suitable to reproduce the rotational curve of the entire thick disk, they show that the presence of an external

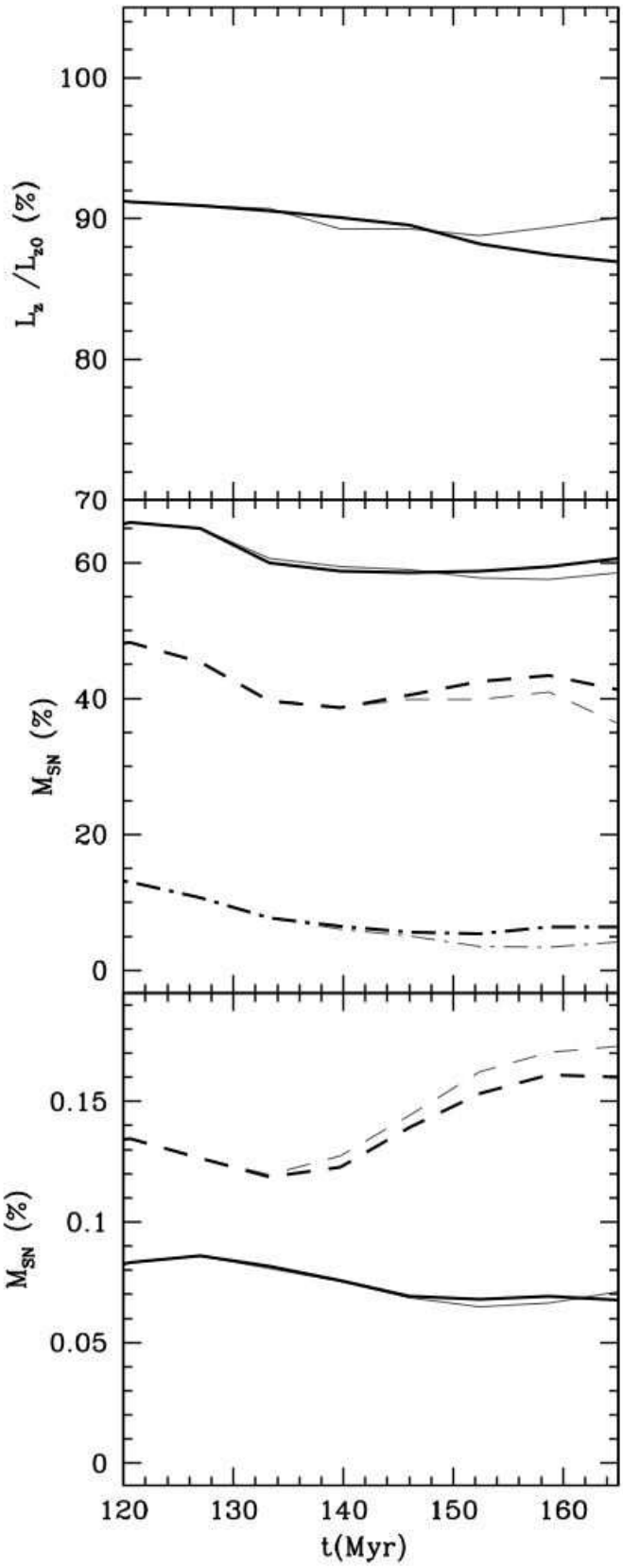

Figure 18. The same as in Fig. 7, but for the cloud model (thin lines) compared with the reference model (thick lines).

gas infall may help to slow down the rotation of the gas in clouds (Fig. 16) and thus the amount of angular momentum that is transferred to the halo. However, higher resolution simulations are still needed in order to explore the role of the K-H instabilities upon the clouds fragmentation and disintegration which have been neglected by Fraternali & Binney (2008) and which are not properly resolved in our simulations.

Finally, we considered the accretion of single, isolated clouds. Our simulations show that this kind of accretion does not alter the general characteristics of the MGFs that arise from the disk.

ACKNOWLEDGMENTS

E.M.G.D.P. acknowledges the partial support from grants of the Brazilian Agencies FAPESP and CNPq.

REFERENCES

Binney J., Dehnen W., Bertelli G., 2000, MNRAS, 318, 658
Boomsma R., Oosterloo T. A., Fraternali F., van der Hulst J. M., Sancisi R., 2008, ArXiv e-prints, 807
Bregman J. N., 1980, ApJ, 236, 577
—, 2004, in Astrophysics and Space Science Library, Vol. 312, High Velocity Clouds, van Woerden H., Wakker B. P., Schwarz U. J., de Boer K. S., eds., pp. 341–+
Brighenti F., Mathews W. G., 1996, ApJ, 470, 747
Cappellaro E., Turatto M., Tsvetkov D. Y., Bartunov O. S., Pollas C., Evans R., Hamuy M., 1997, A&A, 322, 431
Cescutti G., Matteucci F., François P., Chiappini C., 2007, A&A, 462, 943
Chiappini C., 2002, Ap&SS, 281, 253
Croton D. J., Springel V., White S. D. M., De Lucia G., Frenk C. S., Gao L., Jenkins A., Kauffmann G., Navarro J. F., Yoshida N., 2006, MNRAS, 365, 11
de Avillez M. A., 2000, MNRAS, 315, 479
de Avillez M. A., Berry D. L., 2001, MNRAS, 328, 708
de Avillez M. A., Breitschwerdt D., 2005, A&A, 436, 585
Fraternali F., Binney J., Oosterloo T., Sancisi R., 2007, New Astronomy Review, 51, 95
Fraternali F., Binney J. J., 2006, MNRAS, 366, 449
—, 2008, MNRAS, 386, 935
Fraternali F., van Moorsel G., Sancisi R., Oosterloo T., 2002, AJ, 123, 3124
Geiss J., Gloeckler G., Charbonnel C., 2002, ApJ, 578, 862
Hernquist L., 1990, ApJ, 356, 359
Higdon J. C., Lingenfelter R. E., 2005, ApJ, 628, 738
Kahn F. D., 1981, in Astrophysics and Space Science Library, Vol. 91, Investigating the Universe, Kahn F. D., ed., pp. 1–28
—, 1991, in IAU Symposium, Vol. 144, The Interstellar Disk-Halo Connection in Galaxies, Bloemen H., ed., pp. 1–11
Kahn F. D., Brett L., 1993, MNRAS, 263, 37
Koo B.-C., McKee C. F., 1992, ApJ, 388, 93
Korpi M. J., Brandenburg A., Shukurov A., Tuominen I., 1999, A&A, 350, 230
Lacey C. G., Ostriker J. P., 1985, ApJ, 299, 633
Mac Low M.-M., McCray R., Norman M. L., 1989, ApJ, 337, 141
Marcolini A., Sollima A., D'Ercole A., Gibson B. K., Ferraro F. R., 2007, ArXiv e-prints, 708
Melioli C., Brighenti F., D'Ercole A., de Gouveia Dal Pino E. M., 2008, MNRAS, 388, 573
Miller E. D., Bregman J. N., Wakker B. P., 2008, ArXiv e-prints
Navarro J. F., Frenk C. S., White S. D. M., 1996, ApJ, 462, 563
Navarro J. F., Steinmetz M., 1997, ApJ, 478, 13
Palous J., Franco J., Tenorio-Tagle G., 1990, A&A, 227, 175
Raga A. C., de Gouveia Dal Pino E. M., Noriega-Crespo A., Mininni P. D., Velázquez P. F., 2002, A&A, 392, 267
Raga A. C., Navarro-González R., Villagrán-Muniz M., 2000, Revista Mexicana de Astronomia y Astrofisica, 36, 67
Sancisi R., Fraternali F., Oosterloo T., van der Hulst T., 2008, A&ARv, 15, 189
Semelin B., Combes F., 2002, A&A, 388, 826
Shapiro P. R., Field G. B., 1976, ApJ, 205, 762
Spitoni E., Recchi S., Matteucci F., 2008, A&A, 484, 743
Sutherland R. S., Dopita M. A., 1993, ApJS, 88, 253
Takeuchi T. T., Hirashita H., 2000, ApJ, 540, 217
Tomisaka K., 1998, MNRAS, 298, 797
Tornatore L., Borgani S., Matteucci F., Recchi S., Tozzi P., 2004, MNRAS, 349, L19
Toth G., Ostriker J. P., 1992, ApJ, 389, 5
Wakker B. P., York D. G., Wilhelm R., Barentine J. C., Richter P., Beers T. C., Ivezić Ž., Howk J. C., 2008, ApJ, 672, 298
Ward-Thompson D., 2002, Science, 295, 76
Westmeier T., Braun R., Thilker D., 2005, A&A, 436, 101
Wolfire M. G., McKee C. F., Hollenbach D., Tielens A. G. G. M., 2003, ApJ, 587, 278